Bulletin of the Seismological Society of America, Vol. 97, No. 1B, pp. 162–183, February 2007, doi: 10.1785/0120040087

Engineering Ground-Motion Parameters Attenuation Relationships for Greece

by Laurentiu Danciu and G-Akis Tselentis

Abstract Engineering ground-motion parameters can be used to describe the damage potential of an earthquake. Some of them correlate well with several commonly used demand measures of structural performance, liquefaction, and seismic-slope stability. The importance of these parameters comes from the necessity of an alternative measure to the earthquake intensity. In the proposed new attenuation relationship we consider peak values of strong motion, spectral acceleration, elastic input energy at selected frequencies, root-mean-square acceleration, Arias intensity, characteristic intensity, Fajfar index, cumulative absolute velocity, cumulative absolute velocity integrated with a 5 cm/sec^2 lower threshold, and spectrum-intensity energy. This article describes the steps involved in the development of new attenuation relationships for all the preceding parameters, using all existing, up-to-date Greek strong-motion data. The functional form of the empirical equation is selected based on a theoretical model, and the coefficients of the independent variables are determined by employing mixed effects regression analysis methodologies.

Introduction

One of the most important objectives of engineering seismology is to identify critical indices of damage related to key ground-motion parameters. The quantification of ground motion requires a good understanding of the ground-motion parameters that characterize the severity and the damage potential of the earthquake and the seismological, geological, and topographic factors that affect them.

To obtain as accurate a prediction as possible of the level of the anticipated damage, it is desirable to minimize the variability in the correlation between damage index and selected ground-motion parameter. Parameters related solely to the amplitude of the ground motion such as the peak ground acceleration (PGA) are often poor indicators of structural damage. For example, a large recorded PGA associated with a short-duration impulse usually causes less damage than a more moderate PGA associated with a long-duration impulse. In the first case, most of the seismic energy is absorbed by the inertia of the structure with little deformation, whereas in the second case, a more moderate acceleration can result in a significant deformation of the structure.

Because structure or equipment damage is measured by its inelastic deformation, the earthquake-damage potential depends on the time duration of motion, the energy absorption capacity of structure or equipment, number of strain cycles, and the energy content of the earthquake. Therefore, for engineering purposes, parameters that incorporate in their definition the previously mentioned characteristics are more reliable predictors of the earthquake's damage potential. These parameters are: peak ground velocity (PGV), Arias intensity (I_a), a_{rms}, characteristic intensity (I_c), Fajfar's index (I_f), Housner spectrum intensity (SI), acceleration-response spectrum (S_a), elastic input energy (E_i), cumulative absolute velocity (CAV), and cumulative absolute velocity integrated with a 5 cm/sec^2 lower threshold (CAV_5). These ground-motion parameters are defined through equations (1) to (10).

The usefulness of these engineering strong-motion parameters depends primarily on their intended use. Some of them correlate well with several commonly used demand measures of structural performance, liquefaction, seismic-slope stability, etc. For example, for earthquake-resistant purposes, the most important representation of earthquake ground motion is the acceleration-response spectrum, because the acceleration at the natural period of the structure can be multiplied by the mass of the building to estimate the lateral force applied on the structure. One of the major shortcomings of current seismic-design practice, which is based on strength principles (using the acceleration spectrum), is that it does not directly account for the influence of the duration of strong motion or for the hysteretic behavior of the structure. A design approach based on input energy, on the other hand, has the potential to address the effects of the duration and hysteretic behavior directly.

For the purposes of seismic-risk assessment, Wald *et al.* (1999) have developed regression relationships between Modified Mercalli intensity (MMI) and PGA or PGV. These

relationships were used to generate maps of estimated shaking intensities within a few minutes of the event based on the recorded peak motions. These maps provide a rapid visualization of the extent of the expected damages following an earthquake and can be used for emergency response, loss estimation, and public information through the media.

Another application of engineering ground-motion parameters is the development of early warning systems. These systems are low-cost solutions for the reduction of the seismic risk of vital facilities, such as nuclear power plants, pipelines, high-speed trains, etc. The ground-motion parameters and the damage potential threshold are essential for these systems.

If the threshold is set too low, a large number of false alarms question the credibility of the system. If the threshold is set too high, missed or underestimated alarms result in a potentially disastrous false sense of security. Nuclear power plants have long used spectrum acceleration to decide on the shutdown of vulnerable systems after an earthquake. There are several examples where small-magnitude nondamaging earthquakes resulted unnecessarily in shutdowns. These records were characterized by low-energy with high frequency and exceeded the Operating Basis Earthquake (OBE) criteria at high frequency. To prevent this expensive occurrence, the Electric Power Research Institute (EPRI, 1988) found that the best correlation between the onset of damage and ground motion occurred when CAV and I_a measures are used.

For liquefaction, I_a and CAV_5 were found to be the most promising measures of damage potential (Mitchell and Kramer, 2005). I_c and I_f use strong duration information coupled with a cumulative measure of the acceleration record, and they improve the correlation with damage indices. I_c correlates better than a_{rms} with damage and I_f depicts a better correlation with damage than PGV (Riddell and Garcia, 2001).

The objective of this study is to propose new empirical attenuation relationships for the prediction of the engineering ground-motion parameters mentioned earlier instead of those used traditionally for seismic-hazard analysis in Greece, such as maximum or spectral acceleration (Theodulidis and Papazachos, 1992, 1994; Margaris *et al.*, 2002; Skarlatoudis *et al.*, 2003).

Over the past decades several studies have been proposed concerning duration and energy characteristics of ground motion in Greece. Margaris *et al.* (1990) proposed attenuation relationships for bracketed and significant duration. Papazachos *et al.* (1992) studied the bracketed duration of strong ground motion in Greece and proposed a corresponding attenuation relationship. Koutrakis *et al.* (1999, 2002) and Koutrakis (2000) proposed attenuation relationships for Greece based on the bracket duration of ground motion.

Koliopoulos *et al.* (1998) investigated the relationships between duration and energy characteristics of Greek strong ground motion. The predictive relationships based on duration and energy characteristics of strong-motion records were provided in terms of macroseismic information (Modified Mercalli Intensity) or the Housner Intensity Index (Housner, 1952). These relationships are not suitable for seismic-hazard analysis because of their functional form and large errors in the available macroseismic information.

I_a empirical attenuation relations have been presented by Keefer and Wilson (1989), Kayen and Mitchell (1997), Paciello *et al.* (2000), and Travasarou *et al.* (2003). These attenuation relations are, in most cases, similar in form, with magnitude and distance from source to site as the independent variable. The parameters are estimated by statistical fitting of the relationships to the data by means of regression analysis. In a manner similar to the previously mentioned methodologies new empirical attenuation relationships for engineering ground-motion parameters are presented.

Database and Methodology

The strong-motion records used for the study of the attenuation relationships of engineering ground motion have been provided by the European Strong Motion Database (Ambraseys *et al.*, 2004) and presented in Figure 1.

In Greece numerous strong-motion instruments are located in the ground floor or basement of relatively large buildings. In other regions these records are excluded from analysis to minimize the possible bias associated with the effects of such buildings in the measured ground motion. Because in Greece there is a limitation on the availability of good-quality data, it was decided to consider the records from free-field stations and from stations located on the basements of less than two-story buildings. The final dataset consists of 335 records from 151 Greek earthquakes and is presented in Table 1. No correction has been applied to the

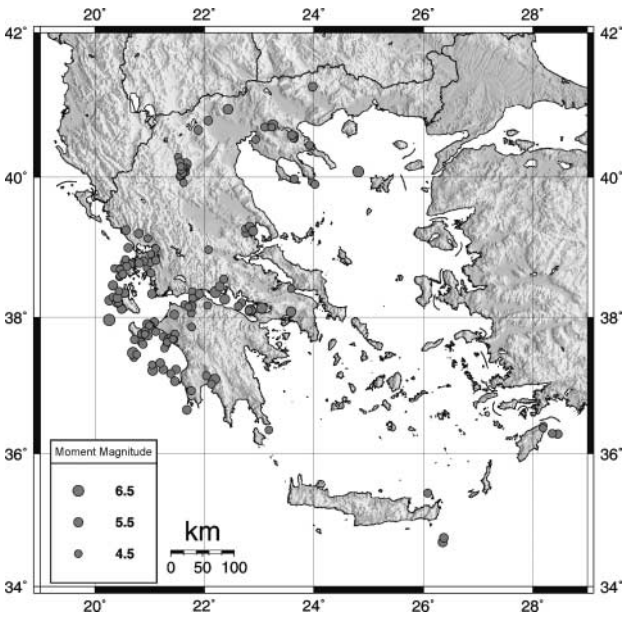

Figure 1. Epicenter distribution of the selected earthquakes.

Table 1
Database of Strong-Motion Records Used in the Regression Analysis

No.	Earthquake Name	Date (dd-mm-yy)	Time	Latitude (°)	Longitude (°)	Moment Magnitude	Focal Depth (km)	Number of Records		
								B	C	D
1	Kefallinia Island	17-09-72	14:07:12	38.245	20.263	5.6	1	0	0	2
2	Ionian	11-04-73	15:52:12	38.78	20.55	5.8	7	1	0	0
3	Ionian	11-04-73	16:11:36	38.76	20.65	4.9	15	1	0	0
4	Patras	29-01-74	15:12:43	38.3	21.86	4.7	13	1	0	0
5	Amfissa	29-12-77	16:52:59	38.55	22.35	5.1	10	1	0	0
6	Volvi	07-04-78	22:23:28	40.7	23.106	5	6	1	0	0
7	Achaia	18-05-78	0:18:49	38.3	21.79	4.5	26	1	0	0
8	Volvi	20-06-78	20:03:22	40.729	23.254	6.2	6	3	1	0
9	Almiros (aftershock)	16-07-80	0:06:58	39.21	22.76	5	12	0	1	0
10	Almiros (aftershock)	26-09-80	4:19:21	39.27	22.75	4.8	5	0	1	0
11	Almiros (aftershock)	08-11-80	9:15:59	39.3	22.83	5.2	5	0	1	0
12	Alkion	24-02-81	20:53:39	38.099	22.842	6.6	10	2	0	0
13	Alkion	25-02-81	2:35:53	38.135	23.05	6.3	8	1	0	0
14	Panagoula	25-05-81	23:04:00	38.71	20.95	4.7	15	1	0	0
15	Levkas	27-05-81	15:04:02	38.79	21.01	5.1	15	1	0	0
16	Preveza	03-10-81	15:16:20	39.2	20.8	5.4	10	1	1	0
17	Paliambela	04-10-81	8:33:32	38.91	21.02	4.7	10	1	0	0
18	Kefallinia Island	17-01-83	12:41:31	37.96	20.26	6.9	5	1	1	0
19	Kefallinia (aftershock)	17-01-83	15:53:57	38.13	20.49	5.2	11	0	1	0
20	Kefallinia (aftershock)	31-01-83	15:27:02	38.12	20.49	5.4	4	0	1	0
21	Kyllini (foreshock)	20-02-83	5:45:12	37.72	21.25	4.9	15	1	1	0
22	Etolia	16-03-83	21:19:41	38.81	20.89	5.2	25	1	0	0
23	Kefallinia (aftershock)	23-03-83	19:04:06	38.78	20.81	5.2	25	1	0	0
24	Kefallinia (aftershock)	23-03-83	23:51:08	38.22	20.41	6.2	3	1	2	0
25	Off coast of Magion Oros peninsula	08-06-83	15:43:53	40.08	24.81	6.6	22	0	1	2
26	Ierissos (foreshock)	14-06-83	4:40:43	40.44	23.92	4.5	10	0	1	0
27	Ierissos	26-08-83	12:52:09	40.45	23.92	5.1	12	0	1	2
28	Near southeast coast of Zakynthos Island	10-04-84	10:15:12	37.64	20.85	5	6	0	1	0
29	Gulf of Corinth	17-08-84	21:22:58	38.21	22.68	4.9	24	1	0	0
30	Arnissa	07-09-84	18:57:12	40.66	21.89	5.2	5	0	1	1
31	Kranidia	25-10-84	14:38:30	40.13	21.64	5.5	20	0	0	1
32	Kremidia (aftershock)	25-10-84	9:49:15	36.93	21.76	5	11	0	0	2
33	Gulf of Amvrakikos	22-03-85	20:38:39	38.99	21.11	4.5	6	0	0	1
34	Anchialos	30-04-85	18:14:13	39.24	22.89	5.6	13	0	1	1
35	Gulf of Kiparissiakos	09-07-85	10:20:51	37.24	21.25	5.4	10	0	0	1
36	Near coast of Preveza	31-08-85	6:03:47	39	20.61	5.2	15	1	2	0
37	Drama	11-09-85	23:30:43	41.26	23.98	5.2	18	0	2	2
38	Aghios Vasileios	18-02-86	5:34:42	40.7	23.23	4.8	3	2	1	1
39	Skydra-Edessa	18-02-86	14:34:04	40.79	22.07	5.3	10	0	1	1
40	Kalamata	13-09-86	17:24:34	37.1	22.19	5.9	1	1	2	1
41	Kalamata (aftershock)	15-09-86	11:41:28	37.03	22.13	4.9	12	0	3	1
42	Tsipiana	02-01-87	5:35:36	37.86	21.77	4.5	20	0	1	0
43	Near northwest coast of Kefallinia Island	27-02-87	23:34:52	38.46	20.33	5.7	5	1	2	0
44	Dodecanese	10-05-87	9:27:02	36.29	28.46	5.3	6	0	1	1
45	Kounina	14-05-87	6:29:11	38.17	22.06	4.6	9	0	1	0
46	Near northeast coast of Crete	02-09-87	12:28:23	35.41	26.08	4.9	18	0	1	0
47	Kalamata (aftershock)	06-10-87	14:50:12	37.24	21.48	5.3	30	1	1	1
48	Near southwest coast of Peloponnes	12-10-87	22:51:14	36.65	21.68	5.2	18	0	0	1
49	Near northeast coast of Rodos Island	25-10-87	13:02:00	36.3	28.36	5.1	10	0	0	1
50	Astakos	22-01-88	6:18:55	38.64	21.02	5.1	10	1	0	0
51	Kefallinia Island	06-02-88	10:35:25	38.32	20.43	4.8	10	0	1	0
52	Gulf of Corinth	04-03-88	3:56:07	38.08	22.82	4.5	5	0	1	0
53	Ionian	24-04-88	10:10:33	38.83	20.56	4.8	1	2	0	0
54	Gulf of Corinth	07-05-88	20:34:52	38.1	22.86	4.9	10	1	1	0
55	Etolia	18-05-88	5:17:42	38.35	20.47	5.3	26	0	2	1
56	Etolia	22-05-88	3:44:15	38.35	20.54	5.4	15	2	2	0
57	Agrinio	03-08-88	11:38:57	38.82	21.11	4.9	28	0	1	1
58	Kyllini (foreshock)	22-09-88	12:05:39	37.93	21.08	5.3	12	0	2	0

(*continued*)

Table 1
Continued

No.	Earthquake Name	Date (dd-mm-yy)	Time	Latitude (°)	Longitude (°)	Moment Magnitude	Focal Depth (km)	Number of Records		
								B	C	D
59	Kyllini (foreshock)	30-09-88	13:02:54	37.69	21.33	4.7	5	1	1	0
60	Kyllini	16-10-88	12:34:05	37.9	20.96	5.9	4	1	5	0
61	Trilofon	20-10-88	14:00:59	40.53	22.94	4.8	20	3	1	1
62	Kyllini (aftershock)	22-10-88	14:58:18	37.88	21.02	4.5	20	1	1	0
63	Kyllini (aftershock)	31-10-88	2:59:51	37.85	21.01	4.8	18	1	1	0
64	Kyllini (aftershock)	27-11-88	16:38:45	37.88	20.99	4.5	8	1	1	0
65	Patras	22-12-88	9:56:50	38.37	21.78	4.9	10	1	2	0
66	Patras	15-05-89	22:40:04	38.28	21.79	4.8	1	0	1	0
67	Patras	31-08-89	21:29:31	38.06	21.76	4.8	23	1	1	0
68	Near southeast coast of Sithonia peninsula	09-03-90	5:35:50	39.93	23.97	4.6	10	0	1	0
69	Aigion	17-05-90	8:44:06	38.39	22.22	5.1	26	0	1	0
70	Near east coast of Zakynthos Island	20-05-90	5:57:24	37.76	20.85	4.5	11	0	1	0
71	Zakynthos Island	24-05-90	18:51:49	37.73	20.97	4.5	1	0	1	0
72	Near east coast of Zakynthos Island	24-05-90	19:59:06	37.8	20.91	4.8	1	0	1	0
73	Plati	08-08-90	0:35:07	37.15	22.04	4.9	10	0	2	0
74	Kefallinia Island	24-08-90	12:54:41	38.24	20.43	4.5	9	0	1	0
75	Near southeast coast of Sithonia peninsula	09-09-90	19:00:39	39.9	24.02	5	1	0	1	0
76	Kefallinia Island	04-10-90	3:19:16	38.21	20.43	4.5	6	0	1	0
77	Griva	21-12-90	6:57:43	40.95	22.43	6.1	1	1	2	3
78	Near southeast coast of Crete	19-03-91	12:09:23	34.673	26.358	5.5	5	0	1	0
79	Near southeast coast of Crete	19-03-91	21:29:27	34.74	26.376	5.2	9	0	1	0
80	Kefallinia Island	26-06-91	11:43:32	38.34	21.044	5.3	4	0	3	0
81	Near north coast of Kefallinia Island	02-01-92	9:05:18	38.29	20.325	4.5	9	0	1	0
82	Kefallinia Island	23-01-92	4:24:17	38.28	20.41	5.6	3	0	3	0
83	Near northwest coast of Kefallinia Island	25-01-92	12:23:23	38.38	20.44	4.5	10	0	1	0
84	Mataranga	30-05-92	18:55:40	38.04	21.45	5.2	12	1	5	0
85	Tithorea	18-11-92	21:10:41	38.26	22.37	5.9	15	1	3	0
86	Pyrgos (foreshock)	14-02-93	10:17:45	37.71	21.38	4.5	4	1	0	0
87	Pyrgos (foreshock)	25-03-93	5:44:09	37.61	21.31	4.5	5	1	0	0
88	Pyrgos (foreshock)	26-03-93	11:45:16	37.68	21.44	4.9	3	3	3	0
89	Pyrgos (aftershock)	26-03-93	12:49:13	37.69	21.42	4.7	10	1	1	0
90	Pyrgos (aftershock)	26-03-93	12:26:30	37.55	21.27	4.5	19	1	0	0
91	Pyrgos (aftershock)	30-03-93	19:08:57	37.64	21.32	4.5	10	0	1	0
92	Gulf of Corinth	02-04-93	2:22:59	38.16	22.62	5	5	1	0	0
93	Off coast of Levkas Island	06-04-93	3:24:27	38.7	20.45	4.8	1	0	1	0
94	Gulf of Corinth	11-04-93	5:18:37	38.34	21.91	5.3	10	1	2	0
95	Pyrgos (aftershock)	29-04-93	7:54:29	37.76	21.46	4.8	0	1	0	0
96	Near coast of Filiatra	03-05-93	6:55:06	37.07	21.46	5.2	1	0	1	3
97	Mouzakaiika	13-06-93	23:26:40	39.25	20.57	5.3	5	2	3	0
98	Patras	14-07-93	12:31:50	38.16	21.76	5.6	13	3	4	0
99	Patras (aftershock)	14-07-93	12:39:13	38.18	21.64	4.6	10	1	2	0
100	Patras (aftershock)	14-07-93	12:54:07	38.15	21.71	4.6	10	1	0	0
101	Pyrgos (aftershock)	07-10-93	20:26:04	37.79	21.11	4.8	10	0	1	0
102	Near southwest coast of Levkas Island	09-10-93	13:33:20	38.58	20.45	4.6	6	0	1	0
103	Off coast of Levkas Island	12-01-94	7:32:57	38.702	20.359	4.6	7	0	1	0
104	Ionian	14-01-94	6:07:48	37.61	20.88	4.9	10	0	1	0
105	Komilion	25-02-94	2:30:50	38.73	20.58	5.4	5	2	3	0
106	Ionian	27-02-94	22:34:52	38.69	20.46	4.8	10	2	1	0
107	Near southwest coast of Levkas Island	15-03-94	22:41:04	38.602	20.459	4.5	0	0	1	0
108	Arta	14-04-94	23:01:34	39.132	20.968	4.5	1	0	1	0
109	Levkas Island	18-07-94	15:44:18	38.626	20.507	4.9	3	0	1	0
110	Paliouri	04-10-94	19:46:21	39.976	23.643	5.1	10	0	1	0
111	Zakynthos Island	17-10-94	9:02:17	37.756	20.912	4.6	14	0	1	0
112	Arnaia (foreshock)	05-03-95	15:39:56	40.541	23.642	4.7	8	0	1	1
113	Arnaia (foreshock)	05-03-95	21:36:54	40.58	23.65	4.6	8	0	1	2
114	Arnaia (foreshock)	04-04-95	17:10:10	40.545	23.625	4.6	9	0	1	1
115	Arnaia	05-04-95	0:34:11	40.59	23.6	5.3	14	0	2	2
116	Kozani	13-05-95	8:47:15	40.183	21.66	6.5	14	0	3	5

(*continued*)

Table 1
Continued

No.	Earthquake Name	Date (dd-mm-yy)	Time	Latitude (°)	Longitude (°)	Moment Magnitude	Focal Depth (km)	Number of Records		
								B	C	D
117	Kozani (aftershock)	13-05-95	11:43:31	40.1	21.6	5.2	10	0	0	1
118	Kozani (aftershock)	13-05-95	18:06:01	40.28	21.52	4.6	29	0	0	1
119	Kozani (aftershock)	14-05-95	14:46:57	40.13	21.66	4.5	0	0	1	0
120	Kozani (aftershock)	15-05-95	4:13:57	40.08	21.65	5.2	9	0	3	1
121	Kozani (aftershock)	16-05-95	23:00:42	40.02	21.56	4.7	0	0	1	0
122	Kozani (aftershock)	16-05-95	23:57:28	40.09	21.62	4.9	0	0	2	0
123	Kozani (aftershock)	16-05-95	4:37:28	40.01	21.58	4.8	9	0	1	0
124	Kozani (aftershock)	17-05-95	4:14:25	40.046	21.58	5.3	10	0	3	1
125	Kozani (aftershock)	17-05-95	9:45:07	40.01	21.56	5	0	0	2	0
126	Kozani (aftershock)	18-05-95	6:22:55	40.03	21.56	4.6	0	0	1	0
127	Kozani (aftershock)	19-05-95	6:48:49	40.09	21.6	5.2	7	0	4	0
128	Kozani (aftershock)	19-05-95	7:36:19	40.06	21.61	4.8	0	0	1	0
129	Kozani (aftershock)	06-06-95	4:36:00	40.14	21.61	4.8	0	0	4	1
130	Aigion	15-06-95	0:15:51	38.362	22.2	6.5	10	1	8	1
131	Kozani (aftershock)	17-07-95	23:18:15	40.21	21.55	5.2	22	0	1	1
132	Kozani (aftershock)	18-07-95	7:42:54	40.101	21.575	4.7	10	0	1	0
133	Aigion (aftershock)	13-08-95	5:17:29	38.101	22.81	4.5	8	0	1	0
134	Kozani (aftershock)	06-11-95	18:51:48	39.92	21.62	4.8	13	0	5	1
135	East of Kithira Island	29-06-96	1:09:03	36.351	23.179	4.5	6	0	0	1
136	Pyrgos	08-11-96	11:43:45	37.684	21.425	4.7	0	0	1	0
137	Zakynthos Island	16-02-97	11:03:19	37.676	20.723	4.9	8	0	1	0
138	Strofades (foreshock)	26-04-97	22:18:34	37.181	21.385	5	7	0	0	1
139	Strofades (foreshock)	29-04-97	23:52:17	37.416	20.713	4.5	2	0	1	0
140	South of Vathi	11-05-97	10:27:56	38.412	23.588	4.6	30	0	3	0
141	Itea	11-05-97	21:10:28	38.44	22.28	5.6	24	0	3	1
142	South of Rhodos	17-07-97	13:21:01	36.412	28.192	4.5	5	0	1	1
143	South of Rhodos	18-07-97	1:45:23	36.38	28.188	4.6	14	0	1	1
144	Varis	22-08-97	3:17:47	40.148	21.572	4.5	23	0	0	1
145	Northwest of Makrakomi	21-10-97	17:57:47	38.971	22.073	4.7	14	0	0	1
146	Strofades	18-11-97	13:07:41	37.482	20.692	6.6	10	2	6	2
147	Strofades (aftershock)	18-11-97	13:13:46	37.229	21.057	6	10	1	3	2
148	Strofades (aftershock)	18-11-97	15:23:35	37.334	21.191	5.3	30	1	1	1
149	Strofades (aftershock)	18-11-97	13:44:05	37.309	21.047	4.8	10	0	1	0
150	Strofades (aftershock)	19-11-97	0:33:07	37.458	20.764	4.8	10	0	1	0
151	Ano Liosia	09-07-99	11:56:51	38.08	23.58	6	17	2	7	0
					Total no. of records			75	197	63

selected records because these records were available in an already corrected form.

A brief description of the dependent and independent variables used to develop the regression analysis is given subsequently. The independent variables consist of those parameters that describe the source, travel path, and site conditions that determine the character and the strength of the ground motion.

The magnitude scale, which we will refer to as M in this article, corresponds to the moment magnitude (Hanks and Kanamori, 1979). For the selected dataset based on data from Greece, M ranges between 4.5 and 6.9.

The regression analysis was performed by using epicentral distance, which we will refer to as R in this article. Because most of the events are offshore, and for those onshore the surface geology does not show often any evident faulting, it is impossible to use a fault distance definition like the closest distance to the fault rupture or to the surface projection of the rupture (Paciello *et al.*, 2000). Hypocentral depths of the selected earthquakes are in the interval 0 to 30 km with a mean of 10.66 km.

The local site classification of each recording station was based on the average shear-wave velocity in the top 30 m of the site (V_{s30}), and presented in Table 2. In this study, 197 recording stations were classified as category C, 63 as category D, and 75 as category B.

Table 2
Definition of Site Categories Used in the Attenuation Models

Site	Categories	Shear-Wave Velocity (m/sec)
B	rock	>800
C	stiff soil	360–665
D	soft soil	200–360

The distribution of the selected dataset with respect to magnitude, distance, and hypocentral depth is illustrated in the Figure 2. Judging from this figure we note that large-magnitude events are recorded at intermediate and long distances and small-magnitude events are observed over small epicentral distances. An exponential trend can be observed and the correlation coefficient between magnitude and distance is 0.64. Based on data distribution, we recommend that the presented attenuation relationships should not be used to predict motions at magnitudes less than 4.5 or greater than 6.9 or epicentral distances greater than 136 km.

The style-of-faulting parameter is used in this study to distinguish between different source types and is classified into three categories. These categories include thrust, strike slip, and normal fault mechanism. For the selected dataset, the records without information regarding style-of-faulting were completed with available information provided by the study of Skarlatoudis *et al.* (2003). Their study empirically demonstrates that the effects of thrust and strike-slip faulting in Greece are similar. Campbell (1981) empirically demonstrated that thrust faulting causes higher ground motion than strike-slip or normal faulting.

In the past, it has been common practice to put strike-slip and normal-faulting events into a single category. However, a recent study by Spudich *et al.* (1999) suggests that normal-faulting events, or strike-slip events in an extensional stress regime, may have lower ground motions than other types of shallow crustal earthquakes.

Engineering ground-motion parameters are the dependent variables that are being estimated in the regression analysis and a short description of these parameters is presented next.

Peak ground velocity (PGV) is, simply, the largest absolute value of velocity in the time series. PGV is less sensitive to the higher-frequency components of ground motion and is more likely than PGA to characterize ground-motion amplitude accurately at intermediate frequencies.

Root-mean-square acceleration (a_{rms}) is a measure of the average rate of energy imparted by the ground motion and is defined as:

$$a_{\text{rms}} = \sqrt{\frac{1}{t}\int_0^t [a(t)]^2 dt} = \sqrt{\lambda_0}, \tag{1}$$

where $a(t)$ is the acceleration time history, and t_s is the total duration of the ground motion.

This parameter is often useful for engineering purposes because it incorporates the effect of duration and it is not strongly influenced by large, high-frequency accelerations, which typically occur only over a very short period. However, a_{rms} does not provide any information about the frequency content because it is the sum of the input energy at all frequencies. Obviously, a_{rms} depends on the method used to define strong-motion duration.

Arias intensity (I_a), as defined by Arias (1970), is the total energy per unit weight stored by a set of undamped simple oscillators at the end of the ground motion. The Arias intensity for ground motion in the x direction (I_{aX}), is calculated as follows:

$$I_{aX} = \frac{2\pi}{g}\int_0^t [a_X(t)]^2 dt, \tag{2}$$

where $a_X(t)$ is the acceleration time history in the x direction, and t is the total duration of ground motion. I_{aX} is a measure of energy, which is scalar in nature, and I_a in the present

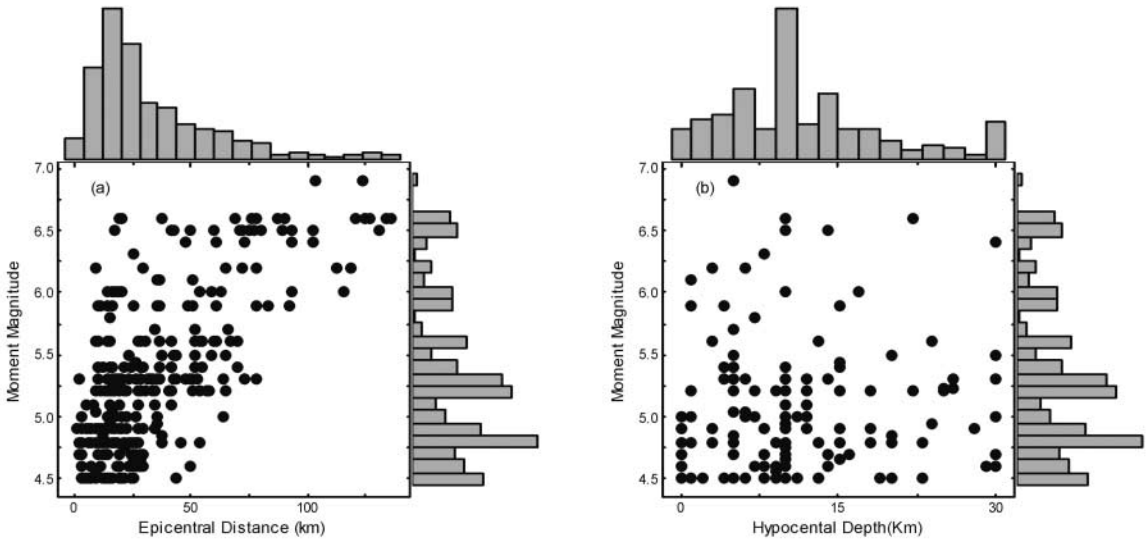

Figure 2. Distribution of the selected datasets in magnitude and epicentral distance (a) and magnitude and focal depth (b).

investigation is considered as the sum of the two horizontal components (east–west and north–south), calculated as follows: $I_a = I_{aX} + I_{aY}$.

Cumulative absolute velocity (CAV) is defined as the integral of the absolute value of ground acceleration over the seismic time-history record:

$$\mathrm{CAV} = \int_0^t |a(t)|\, dt, \tag{3}$$

where $|a(t)|$ is the absolute value of the acceleration, and t is the total duration of the ground motion.

Cumulative absolute velocity integrated with a 5 cm/sec^2 lower threshold (CAV_5) appears to better reflect the longer-period (lower-frequency) components of the motions. Recently, Mitchell and Kramer (2005) proposed the use of CAV_5 as a measure for soil liquefaction. Pore-pressure generation is known to be closely related to strain amplitude, and strain amplitude is proportional to particle velocity, which reflects longer-period components of a ground motion than PGA. This suggests that CAV_5 might have a closer relationship to pore-pressure generation than PGA and I_a. They define:

$$\mathrm{CAV}_5 = \sum_{i=1}^{n} \int_{t_{i-1}}^{t_i} \langle x \rangle |a(t)|\, dt, \tag{4}$$

$$\langle x \rangle = \begin{cases} 0 \rightarrow \text{if } |a(t)| < 0.005g \\ 1 \rightarrow \text{if } |a(t)| \geq 0.005g \end{cases}$$

where t is the total duration of the record, $a(t)$ is the acceleration time history in one-second intervals, where at least one value exceeds the acceleration threshold x and $i = 1$, and n is equal to the record length in seconds.

Characteristic intensity (I_c) proposed by Park *et al.* (1984) is a parameter that has a reasonable representation of the destructiveness of ground motions because correlates well with structural damage expressed in terms of their damage index (Park and Ang, 1985), and is defined as:

$$I_c = a_{\mathrm{rms}}^{1.5}\, t_s^{0.5}, \tag{5}$$

where t_s the significant duration of the ground motion in seconds. Significant duration, t_s, is defined by Trifunac and Brandy (1975) as the interval between the times at which 5% and 95% of the Arias intensity is attained

Fajfar's index (I_f) presented by Fajfar *et al.* (1990) takes into account the PGV and t_s and is defined as:

$$I_f = \mathrm{PGV} \cdot t_s^{0.25}. \tag{6}$$

It has been shown that if this index is used for scaling ground motions, then remarkably different records produce comparable results.

All the preceding parameters depend only on the ground motions. Further they can be classified as peak parameters (PGV), as integer parameters (a_{rms}, I_a, CAV, CAV_5), or combined parameters (I_c and I_f).

Spectrum acceleration (S_a) is the most common response spectral parameter and is related to spectrum velocity (S_v) and spectrum displacement (S_d) by the expression

$$S_a = \frac{2\pi}{T} S_v = \omega S_v = \left(\frac{2\pi}{T}\right)^2 S_d = \omega^2 S_d, \tag{7}$$

where T is the undamped natural period of a single-degree-of-freedom (SDOF) oscillator.

Although S_a provides a convenient tool for specifying an earthquake input, it does not provide information about the duration of strong ground shaking. To correct for this problem, elastic input energy has to be used.

Elastic input energy (E_i) used in this study is the "absolute" input energy proposed by Uang and Bertero (1988) and is defined as:

$$E_i(T) = \max \int_0^t [\ddot{u}(t) + a(t)] v(t) dt, \tag{8}$$

where $\ddot{u}_t(t)$ is the response acceleration of the SDOF system, $a(t)$ is the ground acceleration, $v(t)$ is the ground velocity, and T is the undamped natural period of a SDOF oscillator.

Physically, E_i represents the inertia forces and can be directly related to the sum of the damping and restoring forces or to the total force applied at the base of the structure. E_i can be converted to an equivalent velocity (V_{ei}) by the relationship

$$V_{ei}(T) = \frac{\sqrt{2E_i(T)}}{m}, \tag{9}$$

where m is the mass of the SDOF system. In the present study we use V_{ei} in the regression analysis.

Spectrum intensity (SI) as originally proposed by Housner (1952) may be expressed as the average spectral velocity within the period range [0.1, 2.5], namely,

$$SI = \frac{1}{2.4} \int_{0.1}^{2.5} S_v(T, \xi) dT. \tag{10}$$

The justification given to the integration limits was that they cover a range of typical periods of vibration of urban buildings. Therefore, Housner spectrum intensity may be considered as an overall measure of the capability of an earthquake to excite a population of buildings with a fundamental period between 0.1 and 2.5 sec. The integer interval recommended

by Housner gives good correlation with damage to long-period structures, but poorer correlation with damage of short-period structures. Spectral parameters-period–dependent parameters, presented here, spectrum acceleration, and input energy, were calculated with 5% damping for a total of 31 frequencies in the range between 0.25 and 25 Hz. PGA was introduced in this study to demonstrate the validity of the model, having in mind that for Greece there are no definitive engineering ground-motion parameters empirical attenuation models available today that may be used for comparison.

Using the recorded strong-motion data for these earthquakes, for each horizontal component we computed the previously mentioned ground-motion parameters. The arithmetic average between the two horizontal components of these dependent variables was used to evaluate the attenuation relationships through the regression analysis.

Regression Analysis

Repeated or hierarchical measurements are data in which individuals have multiple measurements over time or space. Analyzing these data requires recognizing and estimating variability both between and within individuals. Further, it is not uncommon for the relationship between an explanatory variable (e.g., magnitude) and a response variable (e.g., PGA) to be nonlinear in the parameters. Nonlinear mixed-effects models provide a tool for analyzing repeated-measurements data by taking into consideration these two types of variability as well as the nonlinear relationships between the explanatory and the response variables. Earthquake data used to develop empirical attenuation relationships can be viewed as repeated measurements, in which the unit of repeated measurement is the earthquake and the epicentral distance plays the role of time.

In the attenuation-relationship situation, the mixed-effects model can be set to reduce the bias introduced if the data are not distributed evenly among the parameters: for example, if magnitude and distance are statistically correlated, or if the data are dominated by many recordings from few earthquakes or recording sites. One approach of the problem is to seek to enhance the estimation of the coefficients of one earthquake from the data available for others. One such way is to introduce a random-effects model.

Brillinger and Preisler (1984, 1985) have proposed a random-effects model to separate the uncertainties associated with between-earthquake (earthquake-to-earthquake) and within-earthquake (record-to-record) variations. Abrahamson and Youngs (1992) introduced an alternative algorithm, which they considered more stable though less efficient. The methods are based on the maximum-likelihood approach.

Nonlinear mixed-effects models involve both fixed effects and random effects. The fixed-effects model for deriving attenuation relationships may be written as:

$$\log(Y_i) = f(M_i, r_i, \theta) + \varepsilon_i, \tag{11}$$

where Y_i is a ground-motion parameter, $f(M_i, r_i, \theta)$ is the attenuation equation, M is the earthquake magnitude, r_i is the distance, θ is a model coefficients vector, and ε_i is the error term for the ith earthquake assumed to be normally distributed with mean zero.

The fixed-effects model is the usual approach for deriving attenuation relationships and the interest is to estimate the model coefficients. Note that the fixed-effects model does not consider the correlation of the distribution of records with respect to individual earthquakes.

The random-effects model presented in equation (12) reduces the bias associated with the distribution of records by including individual random-error terms for within-earthquake and between-earthquake variability:

$$\log(Y_{ij}) = f(M_i, r_{ij}, \theta) + n_i + \varepsilon_{ij}, \tag{12}$$

where Y_{ij} is the ground-motion parameter, $f(M_i, r_{ij}, \theta)$ is the attenuation equation, M is the earthquake magnitude, r is the distance, θ is a model coefficients matrix, ε_i is the error term for the jth records from the ith earthquake, and η_i is the random effect for the ith earthquake.

The ε_{ij} and η_i are assumed to be independent and normally distributed with the variances τ^2 and σ^2, respectively. The intraevent term ε_{ij} represents within-earthquake variability resulting from differences in the data recorded among the different stations for the same earthquake, whereas the interevent term η_i represents between-earthquake variability resulting from differences in the data recorded from different earthquakes. The total standard error for this mixed-effects model is $\sqrt{\sigma^2 + \tau^2}$.

The predictive equation adopted in the present investigation to represent the attenuation of the ground motion has the following form:

$$\log_{10}(Y_{ij}) = a + bM_i - c \log_{10} \sqrt{R_{ij}^2 + h^2} + eS + fF + \varepsilon_{ij}, \tag{13}$$

where Y_{ij} is the response variable (the arithmetic average of the two horizontal components) from the jth record of the ith event, M_i is the moment magnitude of the ith event, R_{ij} is the epicentral distance from the ith event to the location, and h is the "fictitious" focal depth obtained from the regression analysis.

The error term in equation (13) is normally distributed with zero mean and standard deviation σ^2. The dummy variables S and F refer to the site classification and fault mechanism, respectively. Prior to selection of the attenuation model presented in equation (14) we examined the same model with separate terms for soil categories C and D and for separate terms for thrust and strike-slip fault mechanism. Based on the coefficient values, the results suggest that the coefficient values for soil category D is twice the coefficient values for soil category C.

The regression showed that the two coefficients for nor-

mal and strike-slip fault mechanism were almost identical. Therefore, the results indicated that, for the present database, the S can be assumed to take the values: 0 for rock soil (B), 1 for stiff soil (C), and 2 for soft soil (D); and F takes the values: 0 for normal fault mechanism, 1 for both thrust and strike-slip fault mechanism. These later statements are in the agreement with those presented by Skarlatoudis *et al.* (2003).

A nonlinear mixed-effects model (Pinheiro and Bates, 2000) and the procedure given by Davidian and Giltinan (1995) were used to determine the regression coefficients for the empirical models of dependent variables.

A crucial step in the model-building strategy of the mixed-effects model presented in equation (13) is deciding which of the coefficients in the model need random effects to account for their between-earthquake variation and which can be treated as purely fixed effects. The procedure starts with random effects for all parameters and then examines the fitted model to decide which, if any, of the random effects can be eliminated from the model. The near-zero estimate for the standard estimation of one random effect suggests that this term could be dropped from the model and treated as a fixed effect. The Akaike's Information Criterion (AIC) is employed (Akaike, 1974) to compare the models. AIC is a penalized likelihood criterion, and is defined as follows:

$$\text{AIC} = -2 \log \text{likelihood} + k(npar), \qquad (14)$$

where *npar* is the number of the random coefficients in the fitted model, and k is 2 for classical AIC. The value of AIC itself, for a given dataset has no meaning. It becomes interesting when it is compared with the AIC of a series of models specified *a priori*, the model with the lowest AIC being the "best" model among all models specified for the data at hand. For the present mixed-effects model for all the ground-motion parameters the smallest value for AIC criterion was observed when the coefficient "*a*" from equation (14) was treated as a *random effect*. Earthquake magnitude is constant over the records coming from the same earthquake, so the magnitude coefficient b is always treated as fixed to avoid unbalance in the model. Incorrect or inadequate overspecification of the model, can be expected for example, by treating a necessarily fixed parameter as random should lead to computational difficulties (convergence problems).

Coefficient "*h*" is referred to as a "fictitious" depth measure and its values are estimated as a part of the regression. Abrahamson and Silva (1997) and Ozbey *et al.* (2004) have observed that this fictitious depth coefficient provides a better fit to the data at short distances. The soil condition coefficients "*e*" and "*f*" are considered independent of magnitude, distance, and level of ground shaking.

The model was fitted using the conditional linearization method of Lindstrom and Bates (1990), as implemented with the NLME software (Pinheiro and Bates, 2000).

The coefficients of the attenuation model and the variance components, together with their standard errors estimated from the regression analysis, are presented in Table 3. Standard error terms presented in Table 3 show that the aleatory variability in the predictability of I_a and CAV_5 is large. This is not a disadvantage because it has been accepted that I_a has the largest aleatory variability in its prediction compared with the other intensity measures (Travasarou *et al.*, 2003). The smallest value of standard deviation is provided by CAV.

Figure 3 compares the variation of estimated regression coefficients with frequency. The magnitude coefficient b, at the high frequency, is larger for the energy-based parameter V_{ei} than for S_a, suggesting a stronger high-frequency scaling of V_{ei} with magnitude. The distance coefficient c is more positive for V_{ei} than for S_a at almost all frequencies, indicating a disposition for less distance attenuation of V_{ei} than of S_a.

The fictitious depth parameter h appears similar for both parameters for frequencies less than 3 Hz. It is significantly different toward the higher frequencies where h for S_a is larger than h for V_{ei}. The soil category coefficient e seems to be similar for both parameters, V_{ei} and S_a. The fault-mechanism coefficient f for S_a is significantly larger than V_{ei} for frequencies greater than 3 Hz. Finally, the standard error of the regression, σ, decreases with increasing oscillator frequency and is smaller for V_{ei} than for S_a. The results described are for oscillators with 5% damping.

The empirical attenuation relationships for engineering ground-motion parameters for the three soil classifications and magnitude 6.5 are plotted in Figure 4 for comparison purposes. It can be seen that the trend for soft soil to exhibit larger amplitudes than stiff soil and rock is similar for all measures. On Figure 5, it is demonstrated for rock soil that the amplitudes for thrust and strike-slip mechanisms are higher than for normal fault mechanisms. Also the increased amplitudes in integral parameters like a_{rms}, I_a, CAV, and CAV_5 can be partially attributed to the longer duration of earthquake motion associated with soft-soil sites relative to nearby rock sites (Kayen and Mitchell, 1997).

The effects of site geology on the spectral shape of parameters S_a and V_{ei} are presented in Figure 6. The amplification effects of soft soil with respect to stiff and rock are somewhat more important at the short period for the specific values of magnitude (M 6.5) and distance ($R = 10$ km) used in the evaluation of S_a and V_{ei}.

Figure 6 also shows that thrust faults exhibit higher amplitudes for both cases, noting that for S_a this effect becomes negligible at periods greater than about 2 sec. This tendency is consistent with the expectation that thrust and strike-slip fault mechanisms might have on average higher dynamic stress drops than normal fault mechanisms.

Figure 7a,b shows the spectral parameters S_a and V_{ei} calculated at different epicentral distances for a fixed value of magnitude (M 6.5) and fixed-site geology (rock). Figure 7c,d shows the spectral parameters S_a and V_{ei} calculated at a fixed epicentral distance ($R = 10$ km) for three values of magnitude (M 4.5, 5.5, and 6.5) at rock sites.

Table 3
Coefficients and Standard Deviations of Attenuation Model for Engineering Ground-Motion Parameters

$$\log_{10}(Y_{ij}) = a + bM_i + c \log_{10} \sqrt{R_{ij}^2 + h^2} + eS_0 + fF_0 + \varepsilon_{ij}$$

	a	b	c	h	e	f	τ	σ	$\varepsilon_{\text{total}}$
PGA	0.883	0.458	−1.278	11.515	0.038	0.116	0.109	0.270	0.291
PGV	−1.436	0.625	−1.152	10.586	0.026	0.086	0.124	0.283	0.309
l_c	−0.929	0.883	−1.954	10.638	0.030	0.137	0.208	0.426	0.474
l_f	−1.272	0.650	−1.171	11.403	0.023	0.101	0.119	0.281	0.306
l_a	−2.663	1.125	−2.332	13.092	0.028	0.200	0.205	0.482	0.524
a_{rms}	−0.156	0.512	−1.177	10.134	0.026	0.082	0.133	0.264	0.295
CAV	0.015	0.654	−1.163	14.876	0.009	0.103	0.106	0.251	0.272
CAV_5	−1.665	1.138	−2.304	13.470	0.063	0.234	0.183	0.566	0.595
SI	−1.577	0.651	−1.029	9.157	0.031	0.069	0.116	0.294	0.316
S_a (*T*)									
PGA	0.883	0.458	−1.278	11.515	0.038	0.116	0.109	0.270	0.291
0.100	1.544	0.410	−1.364	11.708	0.039	0.112	0.139	0.264	0.299
0.150	1.810	0.429	−1.492	15.721	0.008	0.113	0.107	0.285	0.304
0.200	1.339	0.477	−1.368	14.302	0.024	0.103	0.103	0.287	0.304
0.250	1.126	0.537	−1.443	16.446	0.020	0.109	0.104	0.304	0.321
0.300	0.688	0.582	−1.374	15.117	0.034	0.121	0.107	0.323	0.341
0.350	0.311	0.623	−1.310	14.474	0.037	0.121	0.124	0.323	0.346
0.400	−0.109	0.669	−1.247	12.733	0.033	0.136	0.151	0.322	0.355
0.450	−0.361	0.702	−1.227	11.834	0.019	0.132	0.154	0.322	0.357
0.500	−0.619	0.726	−1.174	10.945	0.021	0.117	0.163	0.318	0.357
0.550	−0.823	0.735	−1.114	9.327	0.020	0.110	0.163	0.322	0.361
0.600	−0.938	0.742	−1.087	8.732	0.011	0.098	0.167	0.321	0.362
0.650	−1.060	0.750	−1.067	8.183	0.013	0.075	0.169	0.323	0.364
0.700	−1.177	0.756	−1.051	7.597	0.020	0.072	0.151	0.329	0.362
0.750	−1.265	0.762	−1.049	7.554	0.030	0.064	0.140	0.330	0.358
0.800	−1.315	0.770	−1.067	7.986	0.024	0.069	0.140	0.331	0.359
0.850	−1.366	0.782	−1.091	8.481	0.019	0.071	0.145	0.326	0.357
0.900	−1.429	0.791	−1.101	8.566	0.016	0.063	0.145	0.325	0.356
0.950	−1.464	0.797	−1.120	8.854	0.014	0.056	0.149	0.321	0.353
1.000	−1.517	0.799	−1.113	9.128	0.016	0.050	0.156	0.314	0.351
1.100	−1.650	0.806	−1.098	9.340	0.025	0.046	0.148	0.307	0.341
1.200	−1.661	0.799	−1.099	10.185	0.023	0.053	0.142	0.303	0.335
1.300	−1.663	0.790	−1.093	10.890	0.015	0.054	0.149	0.299	0.334
1.400	−1.745	0.779	−1.029	10.359	0.013	0.051	0.147	0.296	0.330
1.500	−1.786	0.764	−0.980	9.889	0.011	0.058	0.151	0.291	0.327
1.750	−1.747	0.729	−0.937	10.061	0.008	0.057	0.159	0.278	0.320
2.000	−1.764	0.687	−0.825	9.191	0.009	0.061	0.172	0.267	0.318
2.250	−1.697	0.644	−0.762	8.936	0.010	0.057	0.174	0.271	0.322
2.750	−1.617	0.585	−0.681	8.057	0.008	0.058	0.195	0.270	0.333
3.000	−1.612	0.562	−0.632	6.711	−0.002	0.057	0.205	0.263	0.333
3.500	−1.669	0.534	−0.565	5.347	−0.010	0.064	0.205	0.259	0.330
4.000	−1.834	0.540	−0.573	5.160	−0.007	0.070	0.194	0.258	0.322
V_{ei} (*T*)									
0.100	−0.923	0.566	−1.107	9.560	0.032	0.079	0.125	0.242	0.272
0.150	−0.321	0.527	−1.239	13.542	0.009	0.075	0.099	0.257	0.275
0.200	−0.483	0.541	−1.149	12.459	0.017	0.082	0.116	0.248	0.273
0.250	−0.498	0.563	−1.178	14.649	0.017	0.090	0.114	0.268	0.291
0.300	−0.804	0.600	−1.127	13.098	0.026	0.114	0.127	0.281	0.309
0.350	−1.099	0.643	−1.087	12.420	0.032	0.115	0.143	0.286	0.320
0.400	−1.275	0.672	−1.079	12.238	0.029	0.130	0.140	0.293	0.325
0.450	−1.552	0.712	−1.037	11.139	0.019	0.104	0.146	0.292	0.326
0.500	−1.433	0.700	−1.072	11.609	0.021	0.130	0.143	0.295	0.328
0.550	−1.738	0.732	−1.004	9.502	0.021	0.097	0.153	0.297	0.334
0.600	−1.807	0.734	−0.973	8.658	0.017	0.086	0.155	0.300	0.338
0.650	−1.851	0.741	−0.976	8.661	0.016	0.071	0.154	0.305	0.341
0.700	−1.893	0.744	−0.972	8.284	0.021	0.066	0.146	0.308	0.341
0.750	−1.945	0.754	−0.988	8.362	0.027	0.057	0.145	0.306	0.339
0.800	−1.944	0.755	−0.998	8.646	0.025	0.061	0.142	0.307	0.338
0.850	−1.968	0.762	−1.014	8.877	0.024	0.066	0.137	0.306	0.336

(*continued*)

Table 3
Continued

V_{ei} (T)	a	b	c	h	e	f	τ	σ	ε_{total}
0.900	−2.010	0.765	−1.006	8.661	0.024	0.064	0.138	0.304	0.334
0.950	−2.014	0.768	−1.018	9.141	0.022	0.057	0.144	0.301	0.334
1.000	−2.019	0.769	−1.024	9.543	0.022	0.055	0.148	0.297	0.332
1.100	−2.081	0.776	−1.025	9.778	0.025	0.056	0.142	0.294	0.326
1.200	−2.093	0.769	−1.007	10.198	0.025	0.063	0.137	0.290	0.320
1.300	−2.046	0.755	−0.996	10.311	0.017	0.067	0.138	0.284	0.316
1.400	−2.058	0.744	−0.959	9.900	0.018	0.062	0.133	0.284	0.314
1.500	−2.040	0.730	−0.932	9.401	0.018	0.064	0.131	0.282	0.311
1.750	−1.984	0.704	−0.892	8.846	0.020	0.056	0.134	0.273	0.304
2.000	−1.913	0.676	−0.847	8.594	0.021	0.054	0.143	0.267	0.303
2.250	−1.830	0.649	−0.817	8.133	0.023	0.048	0.137	0.263	0.296
2.750	−1.685	0.615	−0.806	7.958	0.021	0.052	0.137	0.265	0.298
3.000	−1.631	0.602	−0.795	7.523	0.016	0.052	0.135	0.265	0.297
3.500	−1.562	0.585	−0.795	7.264	0.012	0.057	0.130	0.263	0.294
4.000	−1.625	0.606	−0.861	7.721	0.016	0.064	0.122	0.267	0.293

τ and σ represent the inter- and intraevent standard deviation, respectively.

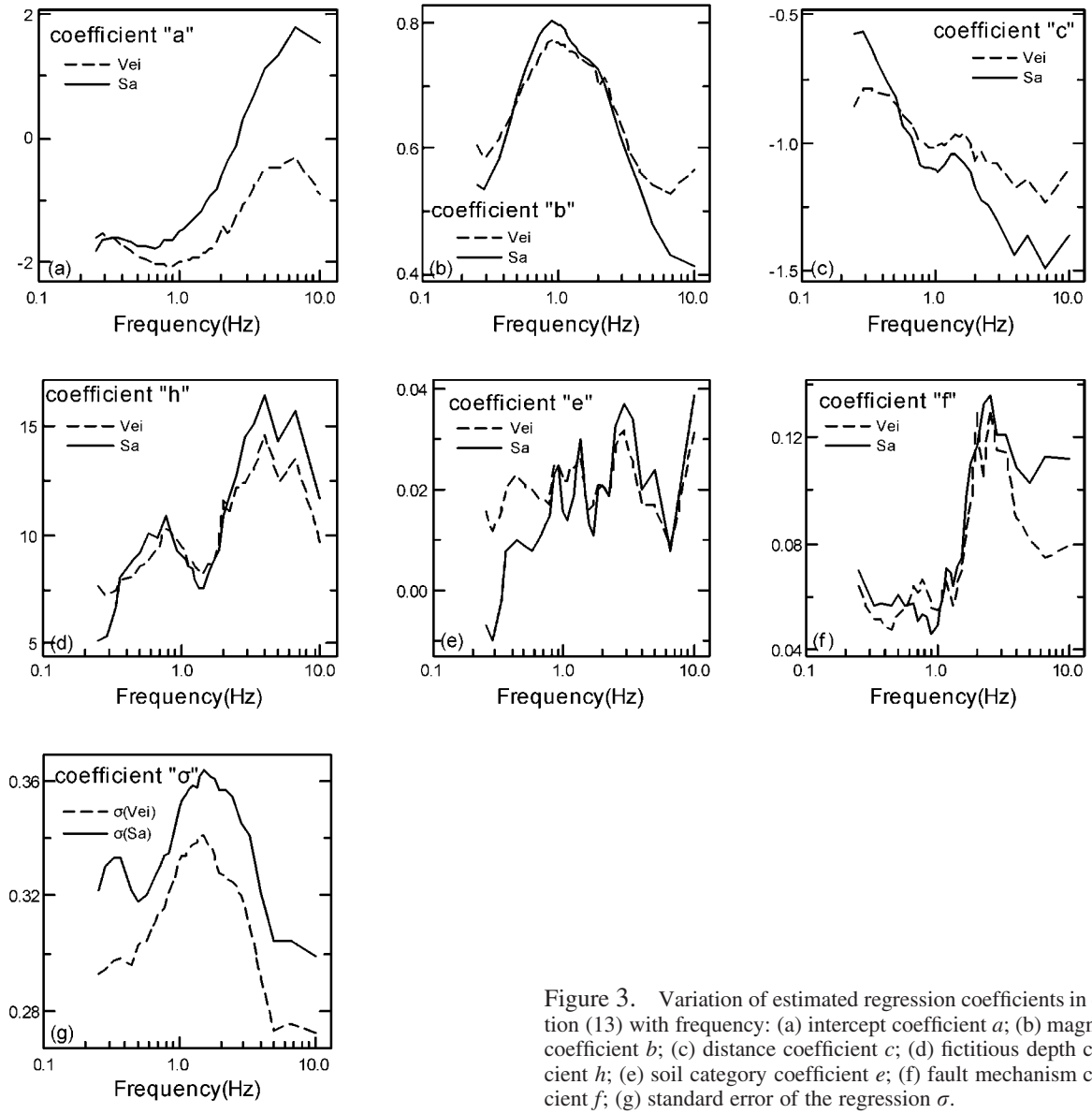

Figure 3. Variation of estimated regression coefficients in equation (13) with frequency: (a) intercept coefficient a; (b) magnitude coefficient b; (c) distance coefficient c; (d) fictitious depth coefficient h; (e) soil category coefficient e; (f) fault mechanism coefficient f; (g) standard error of the regression σ.

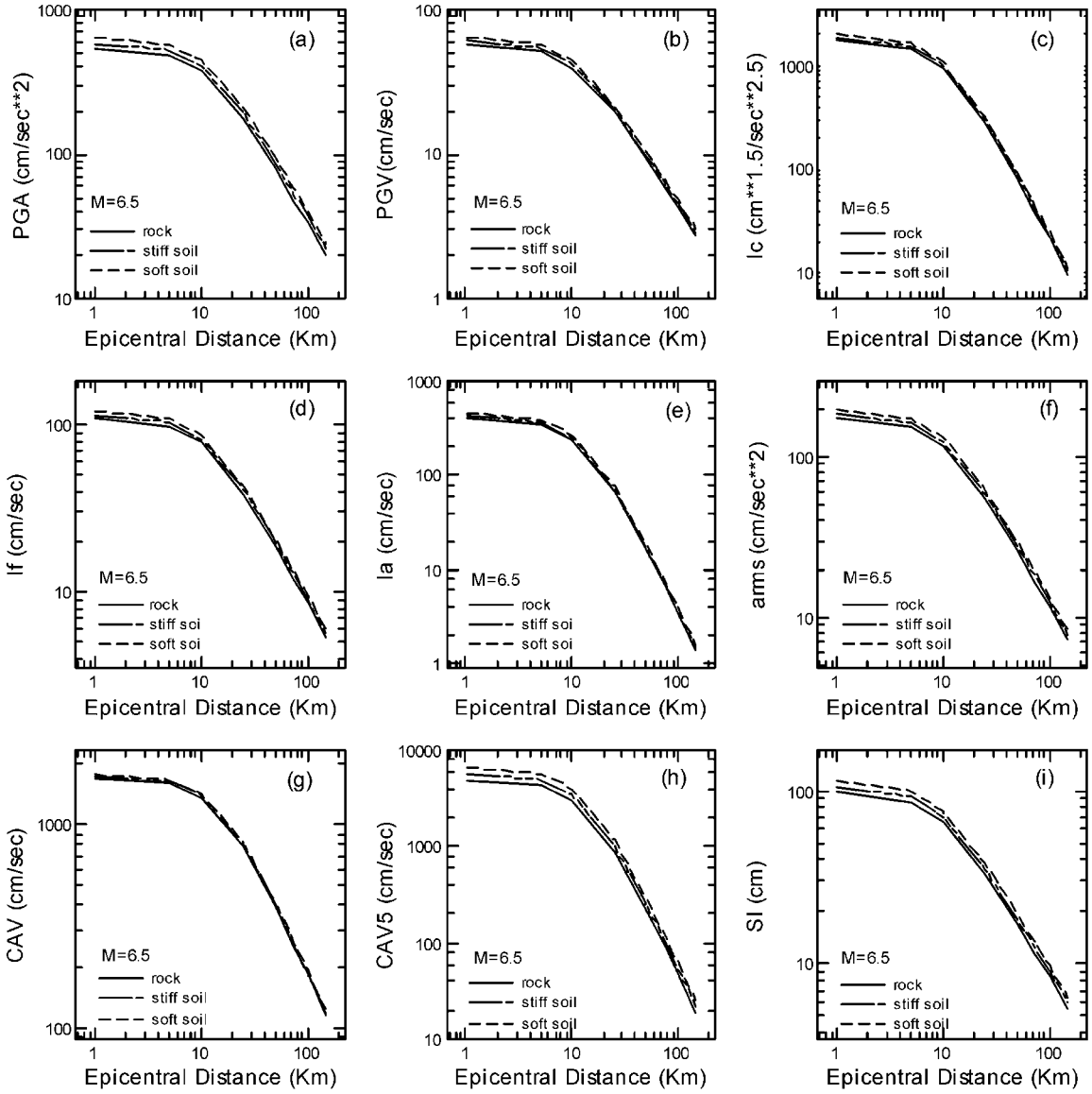

Figure 4. Predicted values of engineering ground-motion parameters as a function of distance and soil category for a fixed moment magnitude M 6.5 and normal faulting mechanism: (a) PGA; (b) PGV; (c) I_c; (d) I_f; (e) I_a; (f) a_{rms}; (g) CAV; (h) CAV_5; (i) *SI*.

The curves have the same shape and the amplitudes decrease with increasing distance in Figure 7a,b and magnitude in Figure 7c,d.

Residual Analysis

The proposed regression models for the engineering ground-motion parameters were validated by means of residual analysis. The inter- and intraevent residuals resulting from the regression analysis were normalized to have a mean zero and a variance of unity. The normalization is done for a better visualization of the differences in the scatter in the residuals among the different ground-motion parameters. For the model to be unbiased, both the inter- and intraevent residuals should have zero mean and be uncorrelated with respect to the parameters in the regression model (Campbell and Bozorgnia, 2003)

The analysis of the residuals resulting from the regression did not show systematic trends as a function of the independent variables used in the model. Moreover, the correlation analysis has confirmed that the residuals were uncorrelated with magnitude, distance, and predicted engineering ground-motion parameters at greater than 99% level of confidence. These observations are similar and valid for all ground-motion parameters considered in the regression model. Because of this similarity in results of the residual analysis only the residual plots for the PGA and S_a at 1 sec natural period are presented here.

Distribution of inter- and intraevent normalized residuals for PGA and S_a ($T = 1$ sec) versus earthquake magni-

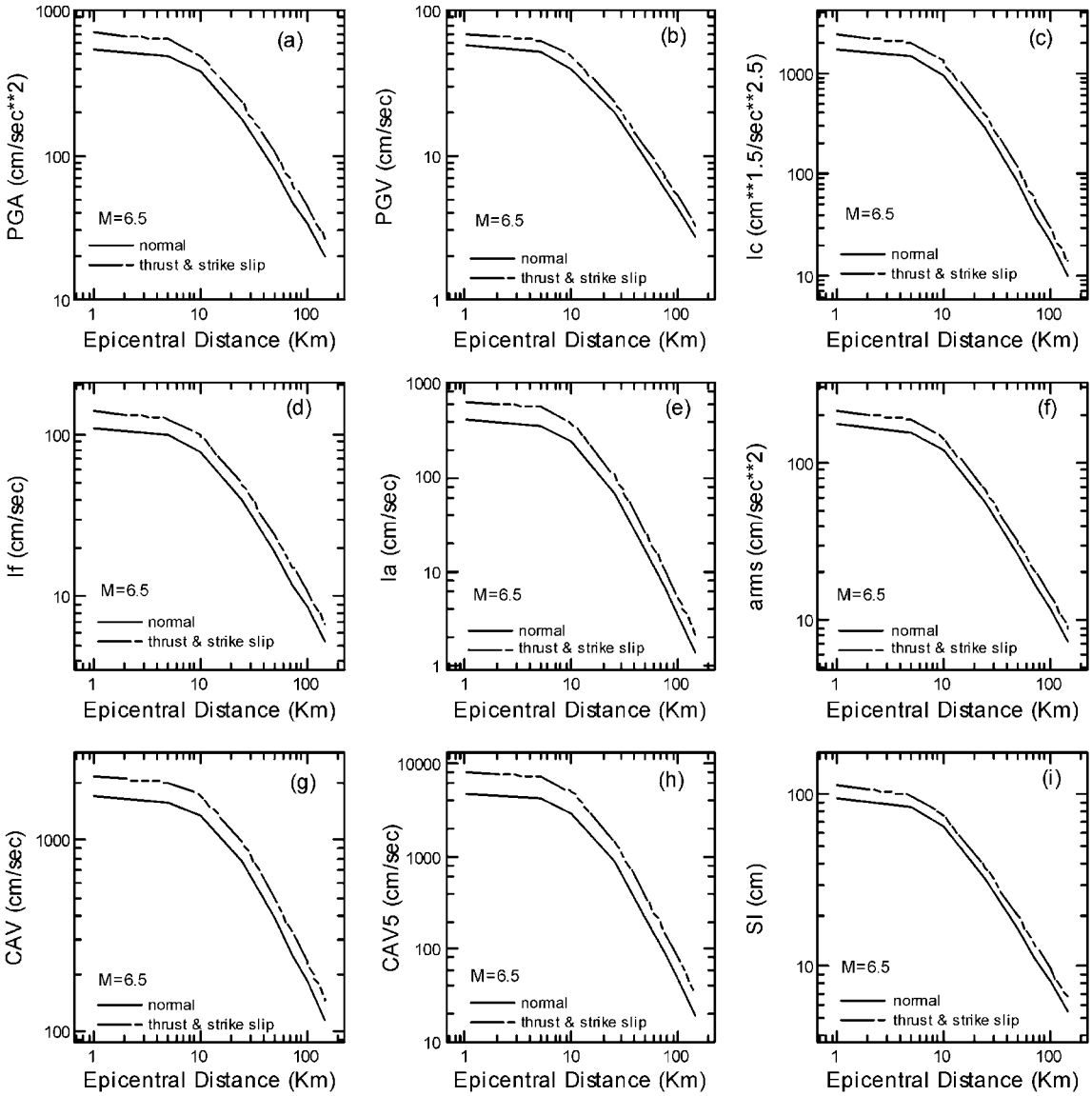

Figure 5. Predicted values of engineering ground-motion parameters as a function of distance and for different fault mechanisms, a fixed-moment magnitude M 6.5, and the rock soil category: (a) PGA; (b) PGV; (c) I_c; (d) I_f; (e) I_a; (f) a_{rms}; (g) CAV; (h) CAV_5; (i) SI.

tude and epicentral distance is presented in Figure 8a,b. A qualitative assessment of normality is obtained by inspecting histograms of the inter- and intraevent residuals of PGA and S_a ($T = 1$ sec) in Figure 9a,b. Inter- and intraevent residuals and the total random error are different among site categories as can be observed in Figure 10a and b. These figures show that the regression models are unbiased with respect to magnitude, distance, site conditions, and faulting mechanism.

Comparison of Proposed Model with Others

For Greece, no engineering ground-motion parameters empirical attenuation models are available today that may be used for comparison. Considering this lack of models, the validity of the model is demonstrated by comparison for PGA predictive equations proposed for the area of Greece. Previously proposed predictive equations of Theodulidis and Papazachos (1992), Margaris *et al.* (2002), Skarlatoudis *et al.* (2003), and Ambraseys *et al.* (2005) were selected for comparison purposes and plotted in Figure 11. All the comparisons presented in this section were computed for epicentral distances ranging from 1 km to 150 km and for a fixed moment magnitude (M 6.5) at rock sites. The proposed relationship is in good agreement with previously proposed attenuation relationships. The shape of the present equation follows a trend similar to the proposed equations and exhibits lower PGA values for short distances.

The difference observed in the near field can be attributed to the fact that we have used the average of the two horizontal components instead of the larger of the two (as

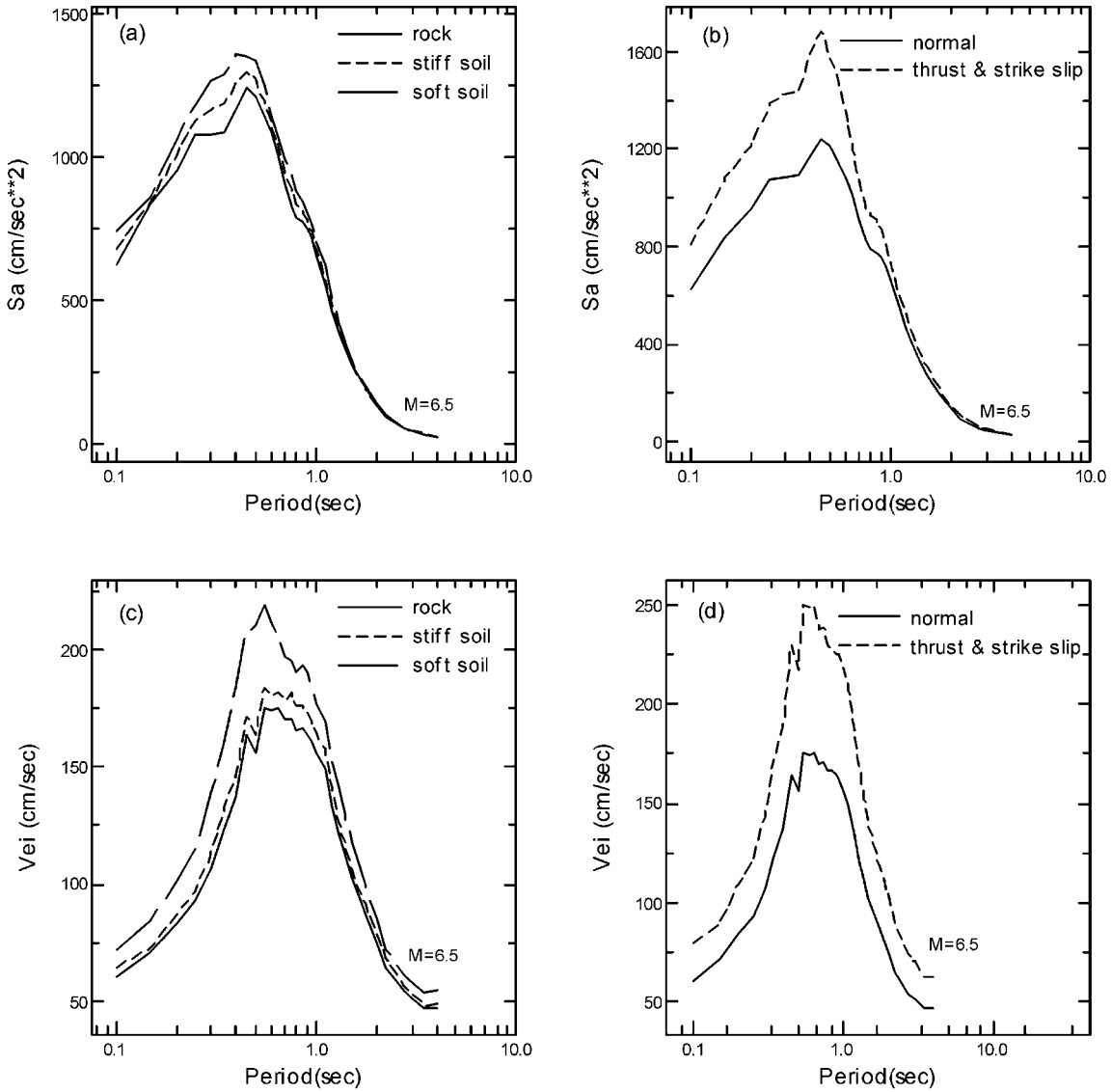

Figure 6. Predicted values of engineering ground-motion parameters for various periods for a fixed-moment magnitude M 6.5 and for a fixed epicentral distance R = 10 km: (a) S_a for different soils and normal fault mechanism; (b) S_a for different fault mechanisms and the rock soil category; (c) V_{ei} for different soils and normal fault mechanism; (d) V_{ei} for different fault mechanisms and the rock soil category.

other authors have), and thus we have introduced some sort of smoothing of data, eventually lowering high values. Also, this discrepancy on the near field can be attributed to the difference in the fictitious depth coefficient. The fact that the fictitious depth coefficient obtained through the regression analysis provides a better fit to the data at short distances was observed by Abrahamson and Silva (1997) and Ozbey *et al.* (2004). The previously mentioned predictive relationships derived from Greek data have been considered in the comparison study for PGV attenuation relationship. The comparison is presented in the Figure 12. The similar trend related to the PGV proposed relations is present and different PGV values for all ranges of distances from 0 to 150 km are observed. Again, the discrepancies in the near field can be assigned to the differences in the fictitious depth coefficient. The equations of Theodulidis and Papazachos (1992) predict consistently higher PGA and PGV values and are probably due to the regression method and the much smaller data used.

Among engineering ground-motion parameters, I_a is the parameter with the greatest number of proposed attenuation relationships. For comparison purposes, in addition to the results of Paciello *et al.* (2000), the equations of Sabetta and Pugliese (1996), Kayen and Mitchell (1997), Travasarou *et al.* (2003), and Bragato and Slejko (2005) are also depicted in Figure 13. Judging from this figure we can see that the predicted Arias intensity is lower than for previously proposed relationships.

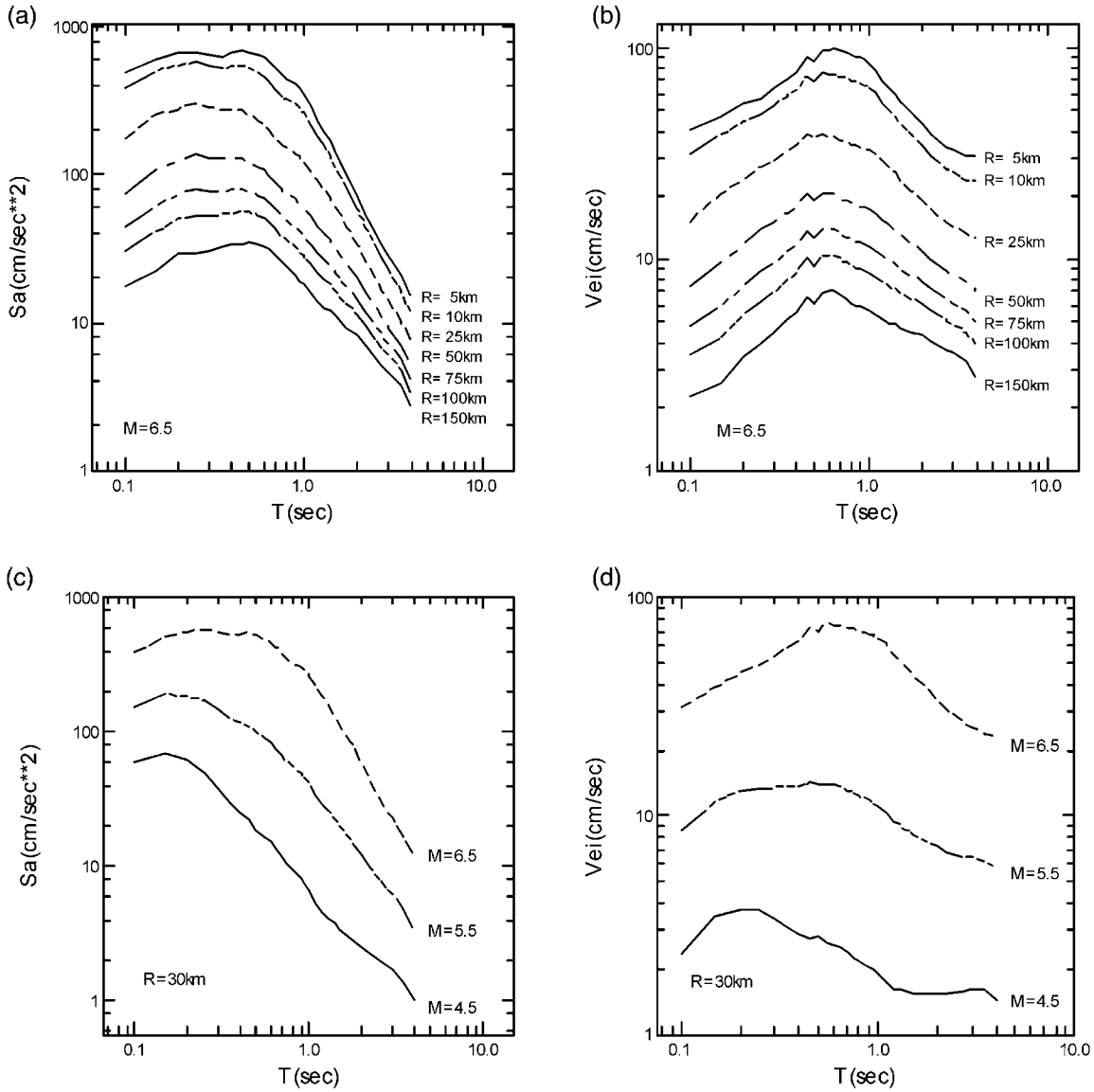

Figure 7. Predicted values at 5% damping versus period and at various epicentral distances of S_a (a) and V_{ei} (b) for a M 6.5 event, normal fault mechanism, and rock soil category. Predicted values at 5% damping versus period for M 4.5, 5.5, 6.5 events, normal fault mechanism, rock soil category, and an epicentral distance of 10 km of S_a (c) and V_{ei} (d).

This can be explained by the different amounts of data that these relationships have been based on, different distance definitions, soil categories, and fault-type definitions. This study used epicentral distance; the same distance is used by Paciello *et al.* (2000) and Sabetta and Pugliese (1996). Travasarou *et al.* (2003) and Bragato and Slejko (2005) used rupture distance and Kayen and Mitchell (1997) used the closest distance to the surface projection of the rupture plane. Alternative definitions of Arias intensity, largest of the two horizontal peaks (Paciello *et al.*, 2000), arithmetic average (present study; Travasarou *et al.*, 2003), or their geometric mean (Bragato and Slejko, 2005) can explain the observed discrepancies.

In Figure 14, we compare the proposed attenuation relationship with that proposed by Mitchell and Kramer (2005) for CAV_5. It can be observed that the two attenuation relationships give different results at short and long distances. At short distances the present CAV_5 curve is slightly higher, whereas for long distances the opposite situation occurs. To explain these differences in the results, we should point out that different data were used. Fifty percent of the data used by Mitchell and Kramer (2005) are from events with moment magnitudes greater or equal than 6. Also, different distance definition (closest distance to the rupture) and the data distribution related to this distance can explain these differences.

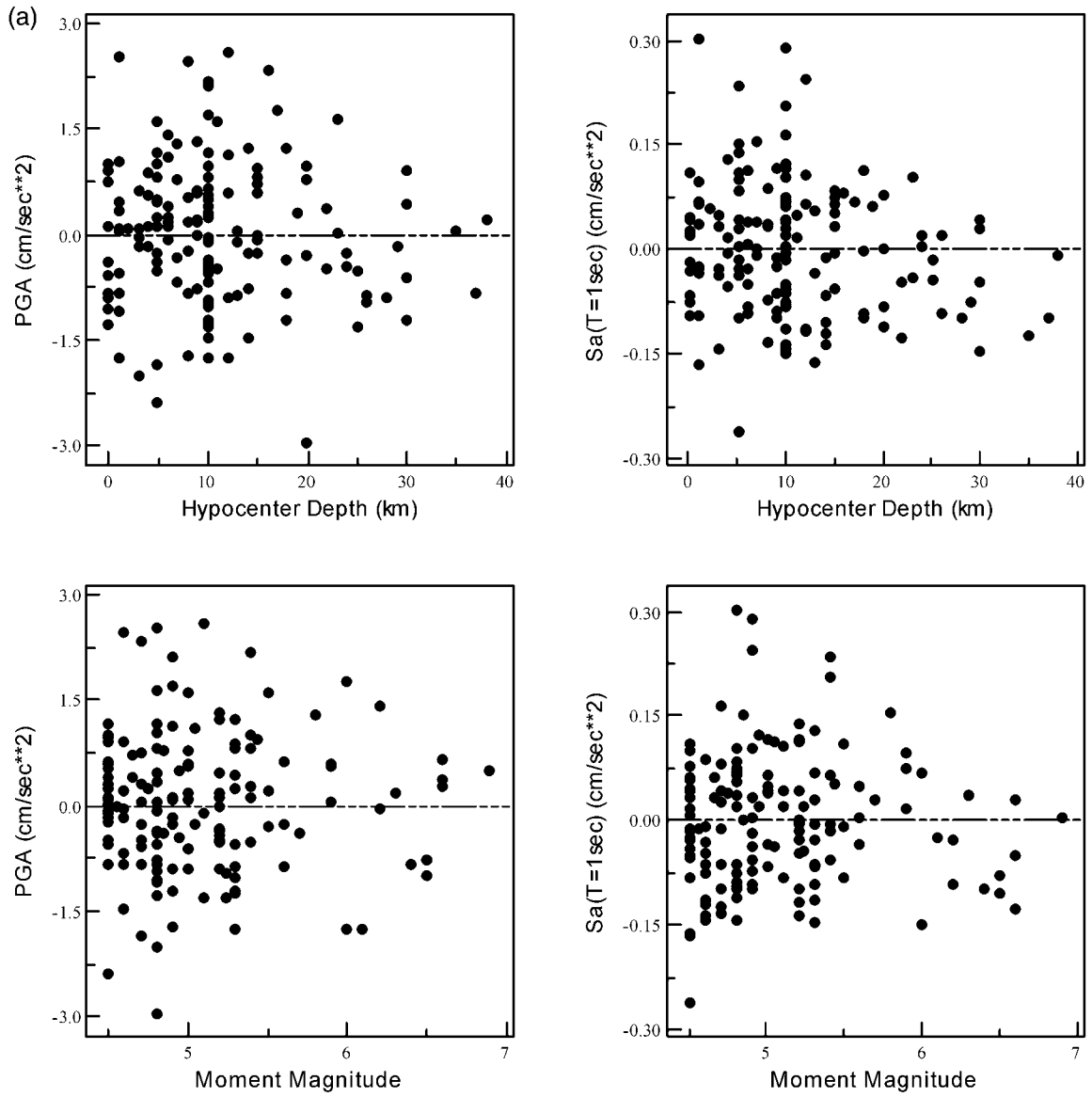

Figure 8. (a) Interevent residuals of PGA and S_a at 1 sec versus hypocentral depth (top left panels) and moment magnitude (top right panels). (*continued*)

The new estimated ground-motion relations for S_a and E_i were compared with ground-motion relations proposed in the studies of Theodulidis and Papazachos (1994) because it is the only single-attenuation relationship available for Greece. The attenuation relationship for S_a is characterized by lack of data. No data for $R < 30$ km and for $M > 6.5$ suggest that a lot of caution is required for using these equations in that range. Thus, comparison between the attenuation relationship for S_a was calculated at fixed epicentral distance ($R = 30$ km) for magnitude 6.5 at rock sites. In addition, widely used relations to estimate S_a proposed by Ambraseys *et al.* (2005) and Sadigh *et al.* (1997) were considered.

Figure 15 compares the predicted S_a from the three selected ground-motion relations with the proposed ground-motion relation. The observed deviation between the present results and those proposed by Theodulidis and Papazachos (1994) can be attributed to the lack of near-field data used by these authors. Furthermore, significant discrepancies are observed between our model and that proposed by Theodulidis and Papazachos (1994) for periods greater than 0.5 sec mainly because of different digitizing and processing procedures. S_a attenuations obtained using equation (13) are similar to those predicted by the equations of Ambraseys *et al.* (2005) and Sadigh *et al.* (1997), except for short periods where our model predicts lower values. This difference could be due to the different definition of distance used here compared with that used by Ambraseys *et al.* (2005) and Sadigh *et al.* (1997).

Comparison of the values for V_{ei} (Fig. 16) predicted by

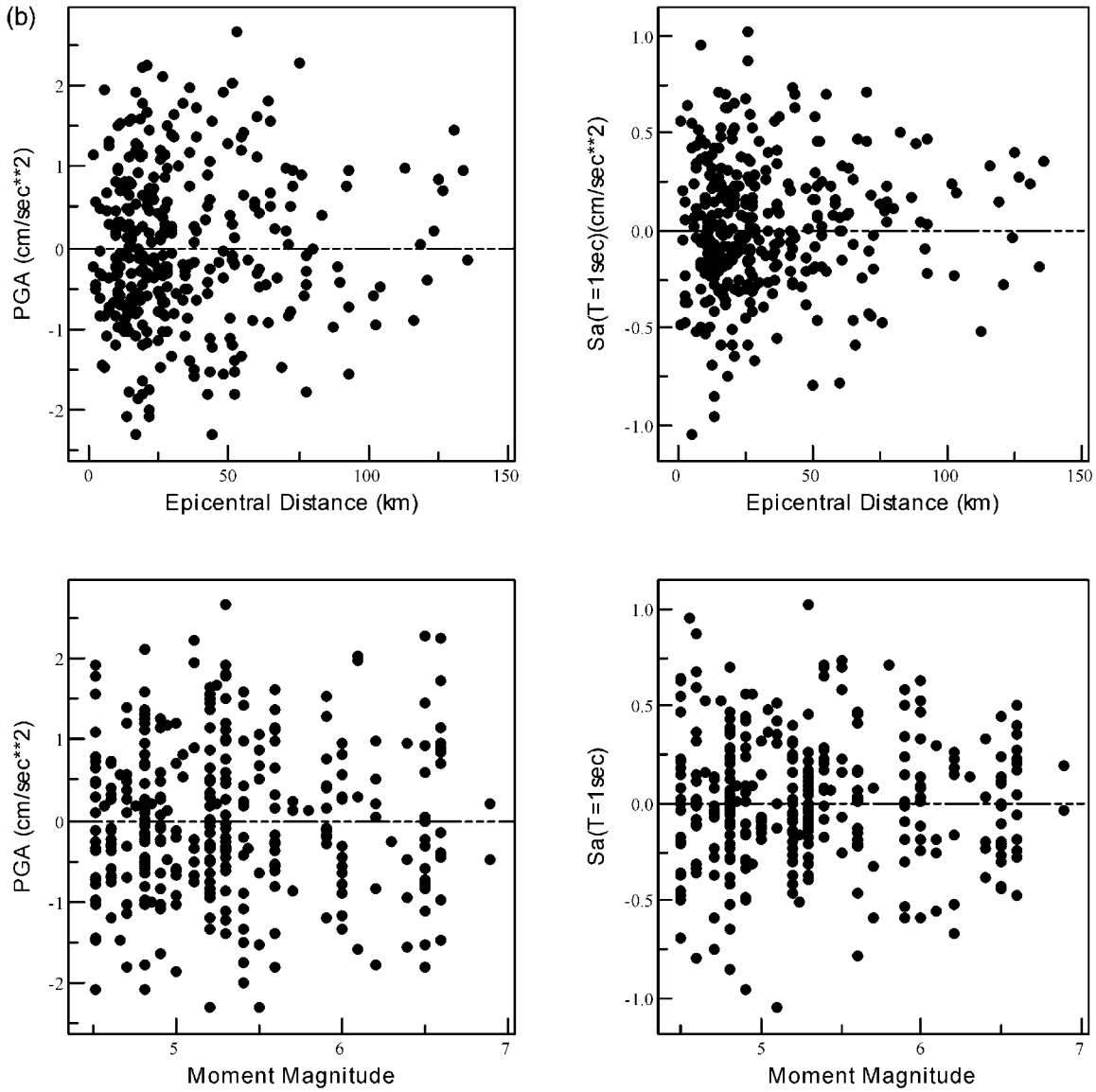

Figure 8. (*continued*) (b) Intraevent residuals of PGA and S_a at 1 sec versus epicentral distance (bottom left panels) and moment magnitude (bottom right panels).

our model with those predicted by the only two attenuation relations for horizontal energy available in the literature (Chapman, 1999; Douglas, 2001) shows similar trends. The peak values of V_{ei} appear at periods in the neighborhood of 0.5 sec for all three relations. V_{ei} predicted by equation (13) shows lower values than those of Douglas (2001) and higher values than those of Chapman (1999).

Conclusions

An attenuation model has been developed for engineering ground-motion parameters for the area of Greece. These categories of engineering ground-motion parameters have the advantage of describing ground-motion damage potential. They capture the effects of amplitude, frequency content, duration, and energy of a ground-motion record. These engineering parameters have been incorporated for the first time in the empirical attenuation relations for Greece. The proposed attenuation relationships could provide an improvement criterion for the selection of earthquake scenarios in terms of engineering ground-motion parameters that are most representative of structural damaging.

Acknowledgments

We thank Tim Sokos and Anna Serpetsidaki at Patras Seismological Lab for their help during the data processing. We want also to thank Gail Atkinson and Bob Youngs for their constructive comments. This research was supported by the Greek State Scholarship's Foundation (IKY) and, in part, by 3HAZ 4043 EC project.

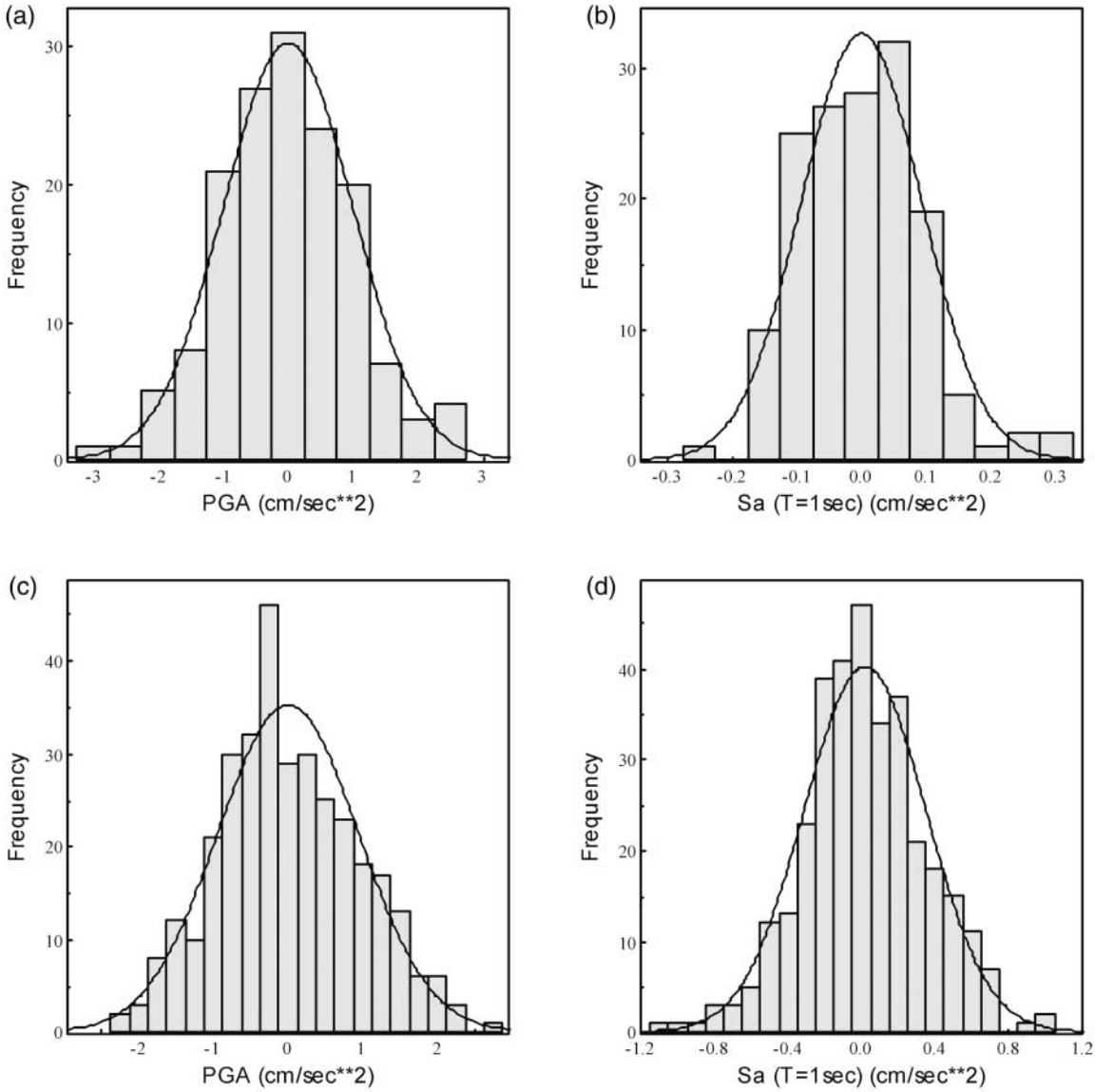

Figure 9. Histogram of interevent of PGA and S_a at 1 sec (a,b) and Intraevent residuals of PGA and S_a at 1 sec (c,d).

References

Abrahamson, N. A., and W. J. Silva (1997). Empirical response spectral attenuation relations for shallow crustal earthquakes, *Seism. Res. Lett.* **68,** 94–127.

Abrahamson, N. A., and R. R. Youngs (1992). A stable algorithm for regression analysis using the ransom effects model, *Bull. Seism. Soc. Am.* **82,** 505–510.

Akaike, H. (1974). A new look at the statistical model identification, *IEEE Trans. Automatic Control* **19,** no. 6, 716–723.

Ambraseys, N., J. Douglas, S. K. Sarma, and P. M. Smit (2005). Equations for the estimation of strong ground motion from shallow crustal earthquakes using data from Europe and the Middle-East: horizontal peak ground acceleration and spectral acceleration, *Bull. Earthquake Eng.* **3,** 1–53.

Ambraseys, N., P. Smit, J. Douglas, B. Margaris, R. Sigbjornsson, S. Olafsson, P. Suhadolc, and G. Costa (2004). Internet-site for European strong-motion data, *Boll. Geofis. Teor. Appl.* **45,** no. 3, 113–129.

Arias, A. (1970). A measure of earthquake intensity, in *Seismic Design for Nuclear Power-Plants*, R. J. Hansen (Editor), MIT Press, Cambridge, Massachusetts, 438–483.

Bragato, P. L., and D. Slejko (2005). Empirical ground-motion attenuation relations for the Eastern Alps in the magnitude range 2.5–6.3, *Bull. Seism. Soc. Am.* **95,** no. 1, 252–276.

Brillinger, D. R., and H. K. Preisler (1984). An exploratory data analysis of the Joyner-Boore attenuation data, *Bull. Seism. Soc. Am.* **74,** 1441–1450.

Brillinger, D. R., and H. K. Preisler (1985). Further analysis of the Joyner-Boore attenuation data, *Bull. Seism. Soc. Am.* **75,** 611–614.

Campbell, K. W. (1981). Near-source attenuation of peak horizontal acceleration, *Bull. Seism. Soc. Am.* **71,** 2039–2070.

Campbell, K. W., and Y. Bozorgnia (2003). Updated near-source ground motion (attenuation) relations for the horizontal and vertical components of peak ground acceleration and acceleration response spectra, *Bull. Seism. Soc. Am.* **93,** no. 1, 314–331.

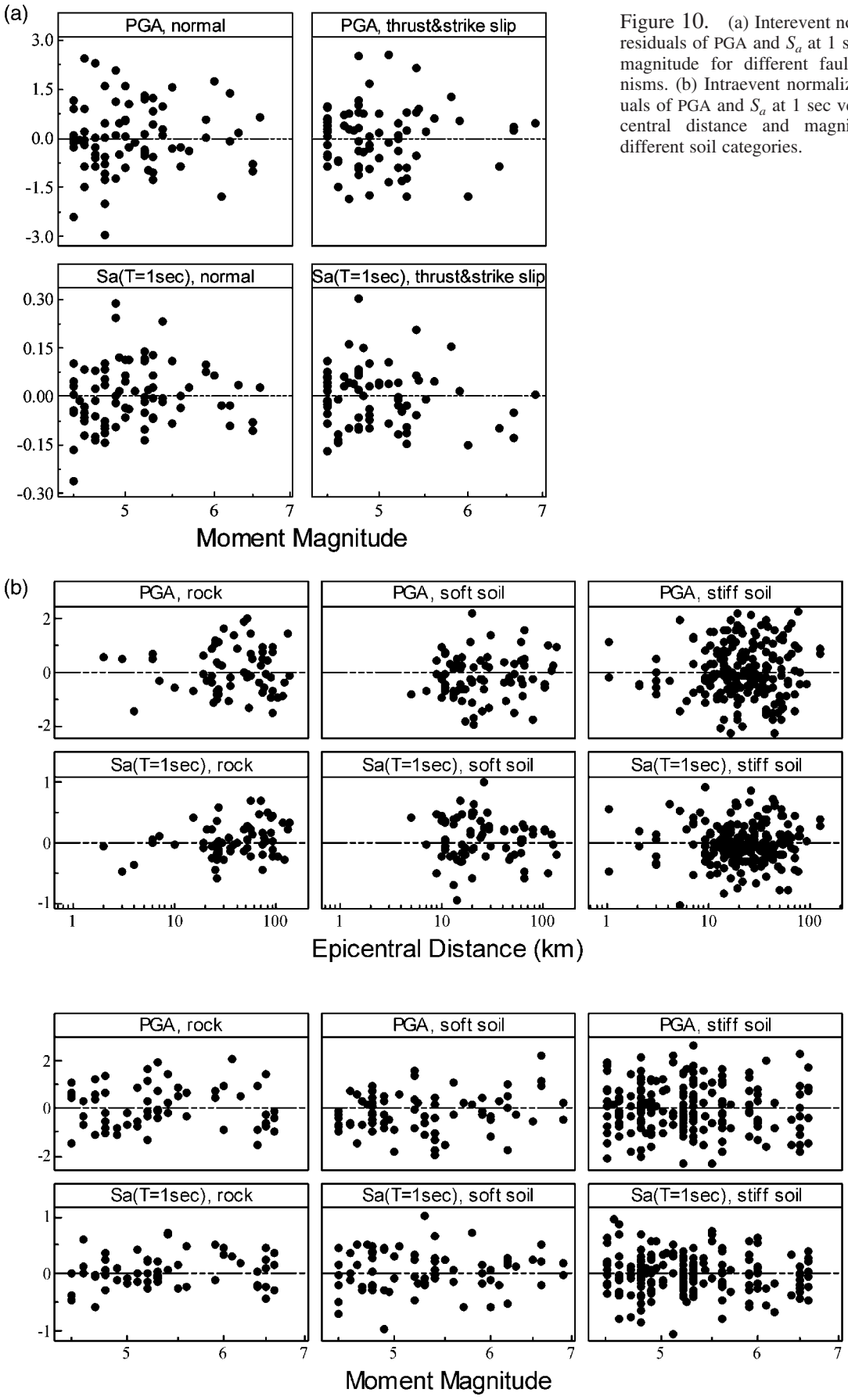

Figure 10. (a) Interevent normalized residuals of PGA and S_a at 1 sec versus magnitude for different fault mechanisms. (b) Intraevent normalized residuals of PGA and S_a at 1 sec versus epicentral distance and magnitude for different soil categories.

2c

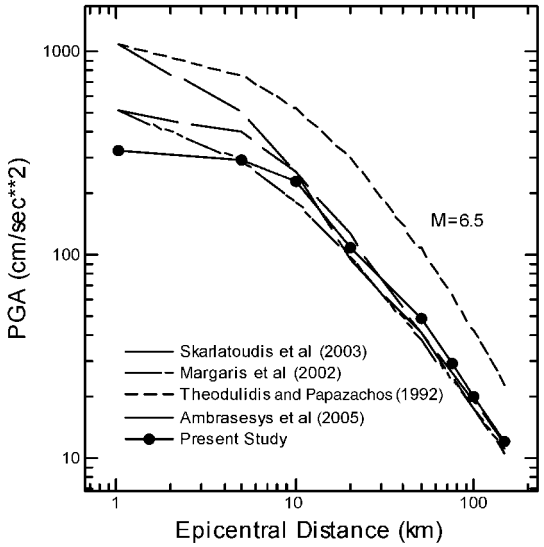

Figure 11. Comparison of the derived PGA attenuation relationship with those proposed by Theodulidis and Papazachos (1992), Margaris *et al.* (2002), Skarlatoudis *et al.* (2003), and Ambraseys *et al.* (2005). The relationships are evaluated for *M* 6.5, normal fault mechanism, and rock soil category.

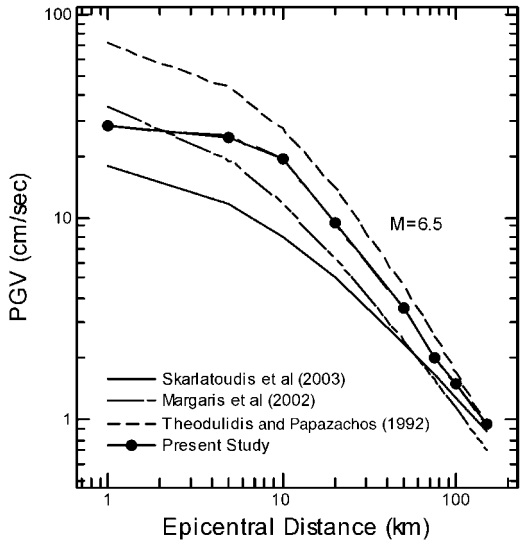

Figure 12. Comparison of the derived PGV attenuation relationship with those proposed by Theodulidis and Papazachos (1992), Margaris *et al.* (2002), and Skarlatoudis *et al.* (2003). The relationships are evaluated for *M* 6.5, normal fault mechanism, and rock soil category.

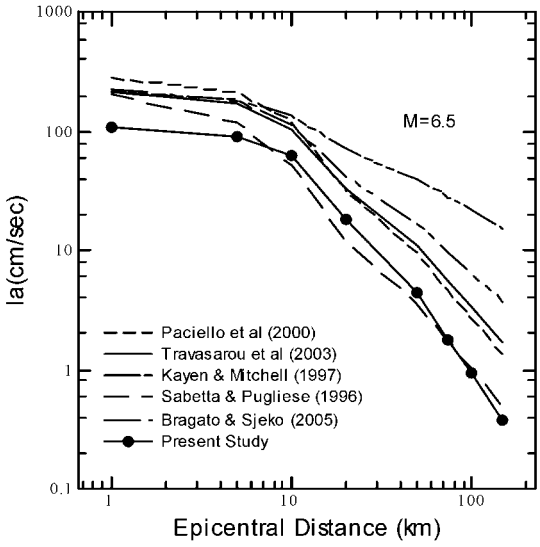

Figure 13. Comparison of the derived I_a attenuation relationship with those proposed by Sabetta and Pugliese (1996), Kayen and Mitchell (1997), Paciello *et al.* (2000), Travasarou *et al.* (2003), and Bragato and Slejko (2005). The relationships are evaluated for *M* 6.5, normal fault mechanism, and rock soil category.

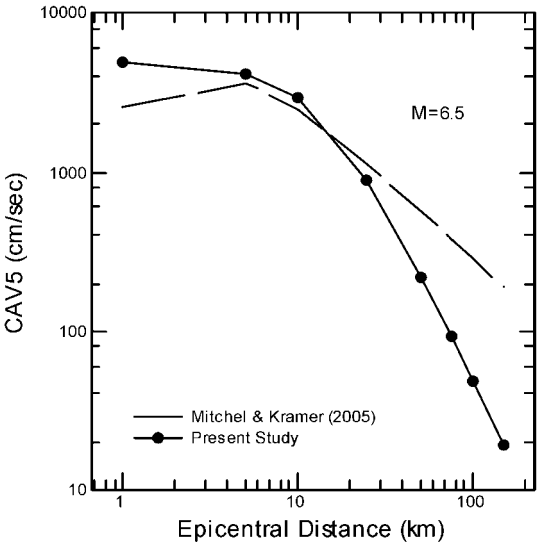

Figure 14. Comparison of the derived CAV_5 attenuation relationship with that proposed by Mitchell and Kramer (2005). The relationships are evaluated for *M* 6.5, normal fault mechanism, and rock soil category.

Chapman, M. C. (1999). On the use of elastic input energy for seismic hazard analysis, *Earthquake Spectra* **15,** no. 4, 607–635.

Davidian, M., and D. M. Giltinan (1995). *Nonlinear Models for Repeated Measurement Data*, Chapman and Hall/CRC, New York.

Douglas, J. (2001). A critical reappraisal of some problems in engineering seismology, *Ph.D. Thesis*, Imperial College, London.

Electrical Power Research Institute (EPRI). (1988). A criterion for determining exceedance of the operating basis earthquake, EPRI NP-5930, Electrical Power Research Inst., Palo Alto, California.

Fajfar, P., T. Vidic, and M. Fishinger (1990). A measure of earthquake motion capacity to damage medium-period structures, *Soil Dyn. Earthquake Eng.* **9,** 236–242.

Hanks, T. C., and T. C. Kanamori (1979). A moment magnitude scale, *J. Geophys. Res.* **84,** 2348–2350.

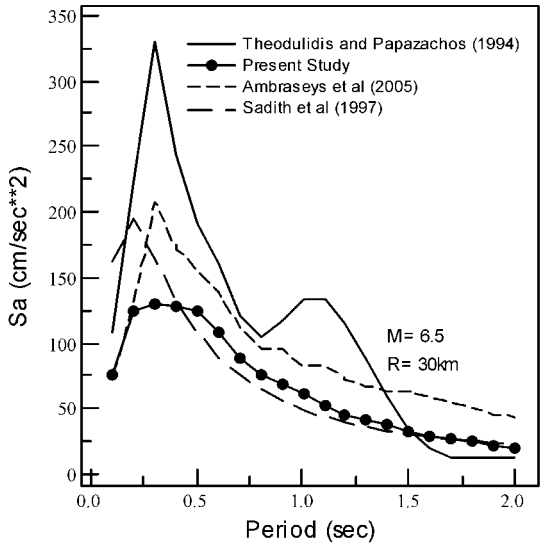

Figure 15. Comparison of the derived S_a attenuation relationship with those proposed by Theodulidis and Papazadios (1994), Ambraseys *et al.* (2005), and Sadigh *et al.* (1997). The relationships are evaluated for M 6.5, normal fault mechanism, rock soil category, and epicentral distance $R = 30$ km.

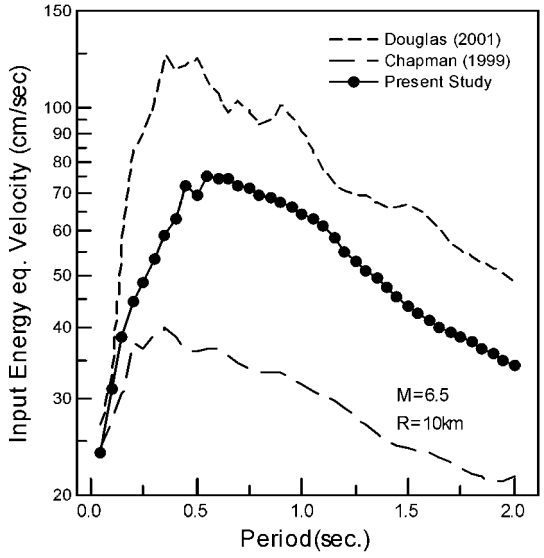

Figure 16. Comparison of the derived V_{ei} attenuation relationship with those proposed by Chapman (1999) and Douglas (2001). The relationships are evaluated for M 6.5, normal fault mechanism, rock soil category, and epicentral distance $R = 30$ km.

Housner, G. W. (1952). *Intensity of Ground Motion during Strong Earthquake*, California Institute of Technology, Pasadena, California.

Kaliopoulos, P. K., B. N. Margaris, and N. S. Klimis (1998). Duration and energy characteristics of Greek strong-motion records, *J. Earthquake Eng.* **2,** no. 3, 391–417.

Kayen, R. E., and J. K. Mitchell (1997). Assessment of liquefaction potential during earthquakes by arias intensity, *J. Geotech. Geoenviron. Eng. (ASCE)* **123,** 1162–1174.

Keefer, D. K., and R. C. Wilson (1989). Predicting earthquake-induced landslides with emphasis on arid or semi-arid environments, in *Landslides in a Semi-Arid Environment*, P. M. Sadler and D. M. Morton (Editors), Vol. 2, Inland Geological Society, San Bernardino, California, 118–149.

Koutrakis, S. I. (2000). A study of the duration of strong-motion in Greece, *M.Sc. Thesis*, University of Thessaloniki, Greece.

Koutrakis, S. I., G. F. Karakaisis, and V. N. Margaris (2002). Seismic hazard in Greece based on different strong motion parameters, *J. Earthquake Eng.* **6,** no. 1, 75–109.

Koutrakis, S. I., V. N. Margaris, P. K. Koliopoulos, and G. F. Karakaisis (1999). New trends in seismic hazard evaluation in Greece, In *Abstracts book, IUGG XXII General Assembly*, Vol. B, Birmingham, 181 pp.

Kramer, S. L., and R. A. Mitchell (2005). Ground motion intensity measures for liquefaction hazard evaluation, *Earthquake Spectra* **22,** no. 2, 413–438.

Lindstrom, M. J., and D. M. Bates (1990). Nonlinear mixed effects models for repeated measures data, *Biometrics* **46,** 673–687.

Margaris, B., C. Papazachos, C. Papaioannou, N. Theodulidis, I. Kalogeras, and A. Skarlatoudis (2002). Ground motion attenuation relations for shallow earthquakes in Greece, in *Proc. of Twelfth European Conference on Earthquake Engineering*, paper ref. 385.

Margaris, B. N., N. Theodulidis, C. Papaioannou, and C. B. Papazachos (1990). Strong motion duration of earthquakes in Greece, in *Proc. XXII Gen. Ass. E.S.C.*, Barcelona, Spain, 865–870.

Ozbey, C., A. Sari, L. Manuel, M. Erdik, and Y. Fahjan (2004). An empirical attenuation relationship for Northwestern Turkey ground motion using a random effects approach, *Soil Dyn. Earthquake Eng.* **24,** 115–125.

Paciello, A., D. Rinaldis, and R. Romeo (2000). Incorporating ground motion parameters related to earthquake damage into seismic hazard analysis, in *Proc. 6th Int. Conf. on Seismic Zonation: Managing Earthquake Risk in the 21st Century*, Oakland, California, 321–326.

Papazachos, C. B., B. N. Margaris, N. Theodulidis, and C. Papaioannou (1992). Seismic hazard assessment in Greece based on strong motion duration, in *Proc. 10th World Conf. Earthquake Engineering*, 425–430.

Park, Y. J., and A. H.-S. Ang (1985). Mechanistic seismic damage model for reinforced concrete, *J. Struct. Eng., ASCE*, **111,** no. ST4, 722–739.

Park, Y. J., A. H.-S. Ang, and Y. K. Wen (1984). Seismic damage analysis and damage-limiting design of R/C buildings, Civil Engineering Studies, Technical Report No. SRS 516, University of Illinois, Urbana.

Pinheiro, J. C., and D. M. Bates (2000). *Mixed-Effects Models in S and S-Plus*, Springer, New York.

Riddell, R., and J. E. Garcia (2001). Hysteretic energy spectrum and damage control, *Earthquake Eng. Struct. Dyn.* **30,** 1791–1816.

Sabetta, F., and A. Pugliese (1996). Estimation of response spectra and simulation of nonstationary earthquake ground motions, *Bull. Seism. Soc. Am.* **86,** no. 2, 337–352.

Sadigh, K., C.-Y. Chang, J. A. Egan, F. Makdisi, and R. R. Youngs (1997). Attenuation relationships for shallow crustal earthquakes based on California strong motion data, *Seism. Res. Lett.* **68,** no. 1, 180–189.

Skarlatoudis, A. A., B. C. Papazachos, B. N. Margaris, N. Theodulidis, C. Papaioannou, I. Kalogeras, E. M. Scordilis, and V. Karakostas (2003). Empirical peak ground-motion predictive relations for shallow earthquakes in Greece, *Bull. Seism. Soc. Am.* **93,** 2591–2603.

Spudich, P., W. B. Joyner, A. G. Lindh, D. M. Boore, B. M. Margaris, and J. B. Fletcher (1999). SEA99: a revised ground motion prediction relation for use in extensional tectonic regimes, *Bull. Seism. Soc. Am.* **89,** no. 5, 1156–1170.

Theodulidis, N. P., and B. C. Papazachos (1992). Dependence of strong ground motion on magnitude-distance, site geology and macroseismic intensity for shallow earthquakes in Greece: I, Peak horizontal acceleration, velocity and displacement, *Soil Dyn. Earthquake Eng.* **11,** 387–402.

Theodulidis, N. P., and B. C. Papazachos (1994). Dependence of strong ground motion on magnitude-distance, site geology and macroseismic

intensity for shallow earthquakes in Greece: II, Horizontal pseudo-velocity, *Soil Dyn. Earthquake Eng.* **13,** 317–343.

Travasarou, T., J. B. Bray, and A. Abrahamson (2003). Empirical attenuation relationship for arias intensity, *Earthquake Eng. Struct. Dyn.* **32,** 1133–1155.

Trifunac, M. D., and A. G. Brady (1975). A study on the duration of strong earthquake ground motion, *Bull. Seism. Soc. Am.* **65,** no. 3, 581–626.

Uang, C. M., and V. V. Bertero (1988). Implications of recorded earthquake ground motions on seismic design of building structures, Report No. UCB/EERC-88/13, Earthquake Engineering Research Center, Berkeley, California.

Wald, D. J., V. Quitoriano, T. H. Heaton, and H. Kanamori (1999). Relationships between peak ground acceleration, peak ground velocity, and modified mercalli intensity in California, *Earthquake Spectra* **15,** no. 3, 557–564.

University of Patras
Seismological Laboratory
RIO 26500, Greece

Manuscript received 2 May 2005.